1 **Holding glycolysis in check though Alox15 activity is required for macrophage M2**

2 **commitment and function in tissue repair and anti-helminth immunity.**

3 Doolan R.[1,2]., Moyat M.[1,3], Coakley G.[1], Wickramasinghe L.[1], Daunt C.[1], Volpe B.[3]., Henkel F.[4,5],

4 Trefzer V.[2], Ubags N.[6], Butler A.[7], Chatzis R.[7], Marsland B.[6,7], Smith A.[8], Deveson Lucas D.[9],

5 McGowan E.N.S.[10], Binger K.J.[11], Esser-von-Bieren J.[4,5] *, Bouchery T.[1,2,3] *[$] and Harris[1,3] N.*

6

7 *[1] Laboratory of Intestinal Immunology, Department of Immunology and Pathology, Monash*
8 *University, Melbourne, VIC 3004, Australia*

9 *[2] Helminth Immunology, Department of Swiss Tropical and Public Health Institute, 4123*
10 *Allschwill, Switzerland; Basel University, 4001 Basel, Switzerland*

11 *[3] Global Health Institute, École Polytechnique Fédérale de Lausanne (EPFL), Lausanne 1015,*
12 *Switzerland*

13 *[4] Center of Allergy and Environment (ZAUM), Technical University of Munich and Helmholtz*
14 *Center Munich, 80802 Munich, Germany.*

15 *[5] Department of Immunobiology, Université de Lausanne, 1066 Epalinges, Switzerland.*

16 *[6] Faculty of Biology and Medicine, University of Lausanne, Service de Pneumologie, CHUV,*
17 *CLED_02.206, Chemin des Boveresses 155, 1066 Epalinges, Switzerland.*

18 *[7] Department of Immunology, School of Translational Medicine Monash University Melbourne*
19 *VIC Australia.*

20 *[8] Friedrich Miescher Institute for Biomedical Research (FMI), Basel, Switzerland.*

21 *[9] Monash Bioinformatic platform, Monash University, Melbourne, VIC 3004, Australia*

22 *[10] The Walter and Eliza Hall Institute, Parkville, VIC 3052, Australia*

23 *[11]Department of Biochemistry and Chemistry, La Trobe Institute for Molecular Science, La*
24 *Trobe University, Bundoora, VIC 3086, Australia*

25 *equal contribution

26 [$] corresponding author

27

28

29

Abstract

Macrophage polarization by type-2 cytokines is central to anti-helminth immunity and tissue repair. While some hallmark changes in macrophages are well-characterized and associated with protection against helminths, it is still unclear how macrophages exert their anti-helminth effects. In this context, we investigated Arachidonate 15-lipoxygenase (Alox15), a lipoxygenase well known for its role in macrophage polarization in the context of metabolic diseases, and a hallmark of type-2 macrophage (M2) human polarization. We show that in the absence of Alox15, M2 cannot trap and kill helminths. Surprisingly, expression of M2 markers was normal despite a loss of function. Instead, we found a concomitant increase in pro-inflammatory responses due to an uncontrolled activation of glycolysis. We further show that activation of Peroxisome proliferator-activated receptor- delta (PPAR-δ) by lipids downstream of Docosapentaenoic acid (DPA) can restore normal glycolysis control, highlighting a novel role for lipids in the fine-tuning of the metabolic support required for optimal macrophage polarization.

Intro

Helminths are large multicellular organisms that have co-evolved with their host displaying very complex host-pathogen relationships. Because of this, despite rarely causing mortality, helminths cause a high morbidity level, especially in tropical and subtropical areas with lower economic status, where burdens are still high[1]. Despite intensive research, to date, there is no vaccine for helminth infections of humans and our understanding of protective responses against re-infection are still incomplete. Laboratory models of the three main type of helminthiases (soil transmitted helminth (STH), filariasis and schistosomiasis) have shown that communication between the adaptive and innate immune systems is required for such protection to occur. Macrophages, in particular, have been shown to be central to protective immune responses against helminths in various murine models, such as filariae and STH [2, 3]. Alternative or "M2" activation triggered by the type 2 cytokines IL-4 and IL-13, by the parasite itself, or by specific antibodies, have been shown to be required to control parasite motility and survival [4-6]. These M2 macrophages express several STAT6-induced effector molecules such as Arginase 1 (Arg1), Resistin-like molecule alpha (Relm-α, Retnla) and chitinase-like protein Ym-1 (Chil3) that have been suggested

59   to contribute to host defense against helminths. Our group and others have described a role for

60   Arginase-1 in protection in rodent hookworm models [4-6]. In other parasite, such as Leishmania

61   Arg1/nitric oxide synthase 2 (Nos2) balance is thought to be crucial for protection [7, 8].

62   Interestingly, a recent paper challenged the importance of Arginase-1 in protection against

63   helminth [9] and this is line with our own observations that treatment blocking Arginase-1 activity

64   was only partially reversing protection [4]. Altogether this prompted us to evaluate other key

65   metabolic molecules in M1/M2 polarization. In an effort to make the finding more translatable

66   (due to high controversy on the importance of Arginase-1 in human macrophages [10]), we looked

67   for key molecules bith highly expressed in human and mouse macrophages polarized by type 2

68   cytokines.

69   In humans, the lipoxygenase Alox15 is highly expressed in response to type 2 cytokines in

70   macrophages both *in vitro* and *in vivo [11-18].* Alox15 is a lipoxygenase that catalyzes the stereo-

71   specific peroxidation of polyunsaturated fatty acids (PUFAs). Alox15 functions to generate

72   phospholipid oxidation products crucial for orchestrating the removal of apoptotic cells as well as

73   synthesizing precursor lipids required for the production of specialized pro-resolving mediators

74   (SPMs) that facilitate the resolution of inflammation [19]. In mice, Alox15 has been implicated in

75   many models of metabolic syndrome such as atherosclerosis, diabetes, obesity, and hypertension

76   [20-22] in which macrophage polarization also plays a key role. Recently, Alox15 has also been

77   shown to be required for the maintenance of alveolar macrophages [23]. Alox15 downstream

78   products are endogenous ligands for the transcription factors PPAR-γ and PPAR-δ [19, 24].

79   In the context of helminth infection, Alox15 and its products have been shown to be upregulated

80   in lung macrophages 7 days post-infection with *N. brasiliensis* and in intestinal tissue during

81   secondary infection with *Heligmosomoides polygyrus [18, 25, 26]*. Furthermore, lipid pathways

82   associated with Alox15 activity have been shown to be increased in macrophages after filarial

83   infection [27]. However, the role of Alox15 in M2 polarization and in protection against helminth

84   has never been addressed to date. In the current study, we demonstrate the crucial role of the

85   Alox15 pathway in M2 polarization through control of a glycolysis:oxidative phosphorylation

86   (OXPHOS) balance and its associated protective role in the context of parasitic infection.

87

Results

Alox15 expression is required for protection against hookworm re-infection

N. brasiliensis (Nb) is a rodent hookworm model that causes long-term activation of IL-4 polarised macrophages in the lungs, through which the parasite migrates on its way to the intestine. Alox15 upregulation in the lungs of Nb infected mice has previously been reported at day 7 (D7) post-infection [25]. We confirmed this upregulation of Alox15 in lung tissue and saw a low but persistent expression of Alox15 transcripts up to D40 post-infection and 2 days post re-infection (Figure S1a). Because Alox15 can be expressed by many cell types, we performed single cell sequencing of CD45+ cells to determine which cell type was principally expressing Alox15 after Nb infection and reinfection (Figure 1a&b). Consistent with the literature, macrophages and T cells are the main cell type that increase in number 40 days post-infection and 2 days post-reinfection. Alox15 expression was specifically increased upon infection in interstitial macrophages (IM), dendritic cells (DC type 1), granulocytes as well as natural killer (NK) cells, with the highest expression in IM. We further validated this increase in macrophage-specific expression of Alox15 by qPCR (Figure S1a).

To explore the role of Alox15 in macrophage polarization in response to a type-2 environment, we utilized Alox15 knock-out mice (Alox15-/-) in which a neomycin resistance cassette has been inserted in exon 3 [28]. It is well-established that upon reinfection with Nb, IL-4 polarised macrophages are able to trap and kill the parasite, resulting in a decreased worm burden in the lungs. We thus assessed the consequence of Alox15 deletion on the protective response against Nb. At 2 days post-reinfection, Alox15-/- mice could not control their infection, with a higher burden of lung larvae as compared to wild-type (WT) controls (Figure 1C). During pulmonary migration, Nb causes extensive damage to the lungs that results in short-term hemorrhage. IL-4 polarized macrophages have been shown to control hemorrhage in both primary and secondary infection [29]. We thus assessed pulmonary hemorrhage and found that hemorrhage 2 days post-reinfection was higher in Alox15-/- mice than in WT counterparts (Figure 1D).

During a primary infection, inflammatory foci and elevated red blood cell levels in bronchoalveolar lavage fluid are resolved by D5. With a classical infective dose of 550 L3, Alox15-/- mice suffered a heightened level of hemorrhage from D3 post-infection, requiring us to

117   lower the dose of infection to avoid adverse events (FigS1b). With a low dose of infection (250

118   L3), equivalent numbers of larvae and hemorrhage were found between WT and Alox15-/- D2

119   post-infection (FigS1c&d). Interestingly, the hemorrhage was not resorbed D5 post-infection in

120   Alox15-/- mice as compared to WT counterparts (Figure 1E). This suggests that the sustained

121   hemorrhage observed 5 days post-infection results from decreased repair rather than enhanced

122   pulmonary damage. IL-4 polarized macrophages contribute to timely wound repair but not the

123   trapping of lung larvae following primary infection [29]. Consistent with a role of Alox15 in IL-

124   4-mediated polarisation of lung macrophages, the intestinal worm burden D5 post-infection was

125   not significantly different between WT and Alox15-/- mice (Figure 1F). Altogether, this suggests

126   that Alox15 is important for both the repair and larvae killing function of IL-4 polarised

127   macrophages.

128

129   **Macrophage Alox15 expression is required for larvicidal activity and tissue repair.**

130   Alox15 is expressed in many cells in the lungs and the impaired tissue repair and larval trapping

131   observed in Alox15-/- mice after primary or secondary Nb infection respectively, could be due to

132   defects in other cell types and involve extrinsic signaling (such as modified eicosanoids in the lung

133   micro-environment) or intrinsic signaling (due to the loss of Alox15 expression in other cells). To

134   determine whether the loss of Alox15 in macrophages alone can recapitulate the loss of protective

135   immunity seen in Alox15-/- mice, we used intranasal adoptive transfer of IL-4 polarised

136   macrophages into naïve mice to mimic the protection usually observed during secondary infection

137   [4]. Wild-type or Alox15-/- bone-marrow derived macrophages were harvested and polarized with

138   IL-4 in vitro to generated M(IL-4) that were transferred intranasally to naïve wild-type animals,

139   which were infected with Nb 1 day later. Mice that received wild-type M(IL-4) had lower worm

140   burdens than those that received Alox15-/- M(IL-4) directly implicating intrinsic Alox15 signaling

141   in the protective response of macrophages to Nb (Figure 2A).

142   Because the mechanisms by which macrophages exert larvicidal effects are incompletely

143   understood, we further explored the importance of Alox15 in larval killing by measuring

144   macrophage-mediated trapping *in vitro* [20]. We setup *in vitro* co-cultures of bone marrow-derived

145   M(IL-4) with Nb third-stage larvae (L3). After 5 days of co-culture, as previously reported [20],

146   wild-type M(IL-4) were bound to Nb L3 (Figure 2 B&C). In contrast, Nb L3 trapping by M(IL-4)

147   generated from Alox15-/- mice was markedly reduced with less macrophages found bound to each

148   larvae (Figure 2 B&C). As heterogeneity in macrophage populations is well established, we

149   validated these findings by isolating pulmonary macrophages by lung digestion and examined their

150   capacity for worm killing. As before, fewer larvae were bound by IL-4 polarized pulmonary

151   macrophages when isolated from Alox15-/- mice compared to WT (Figure 2D). We further

152   assessed if the larvicidal activity of Alox15-/- macrophages was compromised by measuring

153   permeability of the larvae to the cuticle and cell impermeant SYTOX Green dye. In line with the

154   trapping, we observed a marked increase in the percentage of dead larvae trapped by WT

155   macrophages as compared to Alox15-/- (Figure 2E).

156

Alox15 is required for larvicidal activity in an Arginase-1 independent manner.

158   We further explored the role of Alox15 expression in regulating the phenotype of IL-4 activated

159   macrophages. Wild-type or Alox15-/- bone marrow-derived macrophages were generated and

160   polarized with or without IL-4. The expression of canonical M2 signature genes was studied by

161   real-time quantitative PCR (Figure 3A). Despite a strong literature pointing towards the

162   importance of Arginase-1 [4-6] in the anti-helminth role of macrophages, Arginase-1 expression

163   was surprisingly higher in Alox15-/- than in WT M(IL-4) (Figure 3a). MMP-9 gene expression

164   was significantly lower in Alox15-/- M(IL-4) than WT, while other genes typically associated with

165   M(IL-4) polarization (Fizz1, Ym1, Fn1, MMP12, MRC1, TIMP-1) were mostly unaffected by

166   Alox15 deletion. Due to the surprising higher gene expression of Arginase-1 in Alox15-/- M(IL-

167   4), despite a loss of functional parasite killing, we next examined the protein expression and

168   activity of Arginase-1. Arginase-1 expression was slightly higher in Alox15-/- M(IL-4) than WT

169   control (Figure 3B), whilst Arginase-1 activity, measured by urea production, was similar in both

170   WT and Alox15-/- mice (Figure 3C). To assess the relative importance of Arginase-1 and Alox15

171   expression in the anti-helminth function of M(IL-4), we once again set up a co-culture assay of

172   M(IL-4) either from WT or Alox15-/- mice, with or without the addition of the Arginase-1 inhibitor

173   BEC (*S*-(2-Boronoethyl)-l-Cysteine). As previously reported, binding of larvae by wild-type

174   M(IL-4) was reduced by Arginase-1 inhibition (Figure 3D). However, BEC treatment did not

175   further reduce parasite binding by Alox15-/- M(IL-4) (Figure 3D).

176   While Arginase-1 expression is directly triggered by IL-4 stimulation, it has previously been

177   shown that efferocytosis is required for Alox15 gene expression to increase in response to IL-4

178   stimulation [19, 25]. This suggests that Arginase-1 expression could be independent, or upstream,

179   of Alox15 expression. We thus assessed the impact of Arginase-1 blockade on Alox15 expression

180   levels in WT M(IL-4) by immunohistochemistry. We found that Alox15 expression was reduced

181   when Arginase-1 was absent (Figure 3E), suggesting that Arginase-1 expression is upstream of

182   Alox15 and the role of Arginase-1 in M(IL-4) mediated trapping and killing of helminth parasites

183   may occur through indirect pathways [5].

184   Despite several reports of Arginase-1 being required for parasite killing or trapping [4-6], its role

185   in macrophage polarization following IL-4 activation has not been studied in depth. We performed

186   bulk RNA sequencing of WT BMDM treated for 24 hours with IL-4 and/or BEC and compared it

187   to their Alox15-/- counterparts. Surprisingly, only a few genes were significantly downregulated

188   when comparing M(IL-4+BEC) to M(IL-4) and no pathway enrichment could be found. In

189   contrast, 10833 were found to be upregulated by BEC treatment, although many with low fold

190   changes (supplementary table 1). Despite BEC treatment and Alox15 depletion having similar

191   functional consequences both *in vitro* and *in vivo* in terms of loss of parasite trapping/killing, we

192   could not find any genes that were commonly differentially downregulated between the two

193   treatments as compared to M(IL-4) from WT suggesting that Alox15 and Arginase-1 might fall

194   into two distinct anti-helminth pathways or modalities, rather than Alox15 being downstream of

195   Arginase-1.

196   By contrast, we found shared upregulated genes between WT M(IL-4+BEC) and Alox15-/- M(IL-

197   4) as compared to M(IL-4) from WT and performed pathway enrichment analysis in metascape

198   (Figure 3F). The most affected pathways were linked to degranulation, cell motility and antigen

199   presentation, suggesting a possible role in parasite recognition. Interestingly, a few metabolic

200   pathways (lipid metabolism, OXPHOS and TCA cycle) were also significantly upregulated in both

201   BEC treatment and with Alox15 deficiency, suggesting that the loss of function in BEC treated or

202   Alox15 deficient M(IL-4) could be metabolic. Of note, Alox15 expression was 1.26 times

203   upregulated after BEC treatment as compared to WT (log fold change, p-value = 0.06) suggesting

204   a loop of regulation between Alox15 and Arginase-1 expression. Consistent with the findings in

205   Figure 3a, typical M2 polarisation genes were not significantly affected in Alox15-/- BMDM or in

206   BEC treated M(IL-4) as compared to WT M(IL-4).

207

208   Alox15 deficient macrophages have a hybrid pro- and anti-inflammatory commitment after

209   IL-4 polarization

210   To refine our understanding of the role of Alox15 in IL-4 activation of macrophages, we analyzed

211   transcriptomic changes during the transition from resting (M0) to IL-4 stimulated (M(IL-4))

212   BMDM for both WT and Alox15-/- mice. As expected, IL-4 stimulation caused a large number of

213   genes to be up- and down-regulated in WT mice (Supplementary S2a & Table 2). In contrast, direct

214   comparison of M(IL-4) from WT and Alox15-/- mice gave only 19 statistically significant

215   differentially regulated genes (Fig S2b). Metascape was used for enrichment pathway analysis and

216   revealed an enrichment for 'defense response to virus' (GO: 0051607) and 'innate immune

217   response' (GO: 0045087). To refine our understanding of the role of Alox15 in macrophage

218   polarization, we broadened our analysis to the 50 top up- and down-regulated genes between the

219   two genotypes. Interestingly, metabolic and immune processes were found to be affected (Figure

220   S2b). Finally, we looked at the overlap in genes affected by IL-4 treatment between WT and

221   Alox15-/- macrophages. Both genotypes largely overlapped, with 150 shared genes but only 32

222   specific to Alox15 and 21 specific to WT (Supplementary S2c & Table 3). Metascape enrichment

223   pathway analysis revealed the genes specific to WT were enriched for terms linked to cell surface

224   interaction, potentially highlighting a role for worm recognition by macrophages. Surprisingly,

225   genes specific to Alox15-/- were associated with 'inflammatory response' and 'defense against

226   bacteria' (Supplementary S2c& Table 4). Potentially, such differences could explain a difference

227   in the recognition of parasite larvae by IL-4-polarised macrophages from WT or Alox15-/-

228   animals.

229   Optimal activation of 'M2' macrophages, in particular in the context of helminth infection, has

230   previously been reported to require both IL-4 and/or IL-13 stimulation as well as apoptotic cell

231   recognition [25] and is further enhanced by surfactant produced in the lungs [30]. Nb infection

232   causes important damage to the lungs and efferocytosis has been shown to be essential in this

233   model for optimal activation of M2 macrophages [25, 29]. Furthermore, macrophages have been

234   shown to have tissue specificity, with lung macrophages being markedly different from bone

235   marrow-derived macrophages [31]. To validate our findings in the context of helminth infection

236   we assessed the role of Alox15 in IL-4 polarization *in vivo* and performed bulk RNA sequencing

237   on lung macrophages purified 7 days post-infection with *N. brasiliensis* either in WT or in Alox15-

238   /- mice. More marked changes were observed with 1653 genes found to be upregulated and 1073

239   downregulated in Alox15-/- macrophages as compared to WT counterparts (Figure 4a). We next

240   used Metascape pathway enrichment analysis of genes specifically upregulated and downregulated

241   in Alox15-/- lung macrophages. Upregulated genes were associated with immune response

242   pathways characteristic of type 1 responses (response to virus, response to Interferon-beta) (Figure

243   4b). We thus further looked at hallmarked genes typical of 'M2' and 'M1' polarization. As reported

244   earlier, the changes to the M2 phenotype were minor with enhancement of Arginase-1 expression

245   and MMP-9 (figure 4c). In contrast, genes typically associated with M1 polarization were

246   markedly higher in M2 from Alox15-/- mice as compared to WT.

247   As no decrease in hallmark 'M2' genes was observed in M2 from Alox15-/- mice, we conducted

248   pathway enrichment analysis. The downregulated genes specifically associated with Alox15

249   deficiency were linked to cell cycle and cell metabolism (Figure 4d). Association between cell

250   cycle and Alox15 deficiency in macrophages has recently been reported [23], although the authors

251   show that at resting state this defect is limited to alveolar macrophages. Similarly, we only

252   observed this link to cell cycle pathways *in vivo* and not in our RNA sequencing dataset derived

253   from BMDM (Figure S2a-c). To determine whether proliferation contributed to the *in vivo* or *in*

254   *vitro* phenotypes we observed, we assessed proliferation of BMDM from WT or Alox15-/- mice

255   stimulated or not with IL-4. We observed that BMDM stimulated with IL-4 from Alox15-/- mice

256   had no difference in Ki67 expression after one day of IL-4 stimulation. (Fig S2d). We thus

257   concluded that a deficiency in cell cycle was unlikely to explain the lack of larvicidal activity

258   observed in Alox15-/- M(IL-4). Furthermore, given that interstitial macrophages, rather than

259   alveolar macrophages, are required for Nb trapping [4, 32], we decided to further focus on the

260   metabolic changes observed in Alox15-/- lung macrophages. To separate the effect of cell cycle

261   and metabolism we conducted cluster enrichment analysis. The genes downregulated in Alox15-

262   /- lung macrophages formed two separate clusters enriched for cell cycle or metabolic responses

263   respectively. Further pathway enrichment analysis on the latter cluster revealed a strong

264   downregulation of lipid-associated pathways in Alox15-/- lung macrophages (Figure 4e).

265

Alox15 deficient macrophages have a high energetic profile after IL-4 polarization

Polarization of macrophages by IL-4 or IFN-γ has been shown to induce different metabolic requirements [33]. As a main change observed by RNAseq of lung macrophages was linked to metabolic pathways, we further explored the transcriptomic signature of enzymes involved in glycolysis and OXPHOS in lung macrophages of WT or ALOX-15-/- background. In line with the increased expression of M1 polarization genes, genes associated with glycolysis were upregulated in Alox15-/- lung M(IL-4) (Figure 5a). Despite almost no change in IL-4-induced signature genes in Alox15-/- macrophages, genes associated with oxidative phosphorylation – which are typically upregulated by IL-4 – were decreased in our dataset (Figure 5b), as were genes associated with fatty acid oxidation and lipolysis (supplementary Fig S3a&b).

We next wanted to validate whether these gene expression changes translated to altered metabolic phenotypes. Using a Seahorse bioanalyser we compared resting BMDM (M0) to M(IL-4) and M(LPS) from a WT or Alox15-/- background. Even at resting state, Alox15-/- macrophages had a high energetic status with both a high ECAR and high OCR, as compared to WT (supplementary Fig S3c). This difference was even stronger after IL-4 polarization (supplementary Fig S3c). At baseline, there was no difference in spare respiratory capacity (SRC) between WT and Alox15-/- macrophages. However, after IL-4, but not LPS stimulation, there was a marked difference in SRC between the two genotypes, suggesting that Alox15 macrophages were still receptive to IL-4-mediated induction of OXPHOS as has been reported previously for WT mice (Figure 5c).

Interestingly, even from baseline, Alox15-/- BMDM exhibited a higher glycolytic capacity than their WT counterparts (Figure 5d). As expected, stimulation with LPS enhanced glycolysis in WT mice, but not in Alox15-/- macrophages (Figure 5d). Instead, a marked increase in glycolysis could be seen after IL-4 polarization in Alox15-/- macrophages, in an apparent superposition of the two metabolic responses usually attributed to M1 and M2 polarizations.

To investigate if increased glycolysis in Alox15-deficient macrophages was responsible for their lack of anti-helminth function, we polarized BMDM with IL-4 in medium containing either a lower or higher glucose content and examined worm binding as before. Interestingly, when Alox15-/- macrophages were polarized in glucose-limited conditions, cells were able to trap larvae to the

294 same extent as their WT counterparts (Figure 5e). In contrast, WT macrophages polarized in

295 glucose-limited conditions were less efficient at trapping larvae in line with a previous report of

296 poor M2 polarization in low glucose settings (Figure 5e, [32]).

297

Alox15 is central to the anti-helminth activity of macrophages but not in anti-*Leishmania* immunity

300 We found it striking that after LPS polarization, OXPHOS was heightened in Alox15-/-

301 macrophages but that the high baseline glycolysis rate of Alox15 macrophages remained

302 unchanged. We thus decided to further explore the importance of Alox15 in M1/M2 polarization.

303 First, we polarized bone marrow derived macrophages with M2 or M1 stimulants (IL-4, IL-13,

304 LPS and IFNγ) and then co-cultured these cells with Nb. As previously described [34], 'M0'

305 macrophages can to some extent bind to Nb larvae and IL-4 polarization enhances this binding

306 (Figure 6a). Interestingly, the reduced binding of Alox15-/- macrophages was not observed when

307 cells were stimulated with IL-13 alone or IL-13 together with IL-4, suggesting IL-13 polarisation

308 might be Alox15-independent. In line with the literature, 'M1' polarized macrophages, stimulated

309 with LPS or LPS+IFNγ, were unable to bind to Nb larvae when derived from WT mice (Figure

310 6a). Alox15-/- mice exhibited increased binding as compared to M1 macrophages from WT mice,

311 and instead looked similar to M0 macrophages from either strain (Figure 6a). This indicate an

312 overall defect in macrophage polarization in absence of Alox15.

313 Unlike helminths, Leishmania are obligate intracellular parasites. Macrophages act as the

314 replicative niche or clear intracellular parasites, depending on their activation state. Increase ARG1

315 activity is thought to be beneficial to the parasite in several ways. Firstly, ARG1 competes with

316 NOS2 for L-arginine substrate, thereby diminishing NO· and parasite death [35-37]. Secondly,

317 increased availability of L-arginine in non-inflammatory macrophages is diverted into polyamine

318 synthesis. Polyamines are required for parasite growth and production of the antioxidant

319 trypanothione, which assists in withstanding the oxidative environment within the parasitophorous

320 vacuole[35]. ARG1 catalyses the conversion of L-arginine to urea and L-ornithine, a precursor for

321 polyamine species required for Leishmania spp. replication [35-38].

322 Given the mixed M1/M2 polarisation of Alox15 M(IL-4) and higher Arginase-1 expression, we

323 set out to assess if control of this protozoan parasite is similarly affected by Alox15 deficiency.

324 Interestingly, in a low dose model of infection with *L. mexicana*, Alox15 deficiency caused a slight

325 decrease in parasite index at late time points indicating better macrophage control (Figure 6b).

326 Despite this, we did not observe a difference in nitric oxide concentration even at late time points

327 between the two genotypes (figure 6c). We next increased the multiplicity of infection to highlight

328 differences in genotypes. Higher dose infections are more susceptible to a shift in the Arginase-

329 1/iNOS balance. Interestingly, in high dose experiments, no difference between genotypes could

330 be seen at any of the time points (Figure 6d). Polarization with LPS or with IL-4+IL-13 gave

331 similar results (Figure 6d), suggesting that Alox15 is not involved in the control of Arginase-

332 1/iNOS balance, nor is it required for killing of *L. mexicana*.

333 To prove that the phenotype we reported is not just specific to IL-4-mediated polarization of

334 macrophages to a phenotype able to kill Nb larvae, we utilized another rodent helminth parasite,

335 namely *Heligmosomoides polygyrus bakerei* (Hpb). Like Nb, protection against secondary

336 infection requires Arginase-1 expressing macrophages [6]. As Hpb is an enteric nematode

337 granulomas rich in macrophages are typically formed around the larvae within the submucosa of

338 the upper small intestine. However, in contrast Nb, activation of macrophages able to kill Hpb

339 larvae requires antibody activation, rather than IL-4. At 4 and 14 days post-secondary infection,

340 Alox15 deficient animals had a higher worm burden that their WT counterparts (Figure 7a&c).

341 During reinfection, granulomas rich in macrophages are typically formed around the larvae in the

342 duodenum of the small intestine. We therefore assessed granuloma number and composition in

343 WT and Alox15-/- mice. There was a marked delay in granuloma formation in Alox15-/- mice,

344 with significantly fewer granulomas in Alox15-/- mice than their WT counterparts 4 days post-

345 reinfection (Figure 7b&d). Of note, parasite burden in primary infection was not different between

346 genotypes (Figure S4a). In line with our findings for Nb infection, the granulomas were still rich

347 in macrophages and expressed heightened level of Arginase-1 in Alox15-/- mice (Figure 7e). As

348 Alox15 can be expressed by other cells that could be involved in the granulomas (eosinophils and

349 epithelial cells), we next used an *in vitro* system to assess the role of Alox15 in macrophage

350 trapping of Hpb larvae. We again generated BMDM and co-incubated them with Hpb L3 in the

351 presence of serum from infected mice, but without IL-4 activation. In line with the phenotype of

352 decreased trapping with Nb, the motility of the larvae co-incubated with (immune serum activated)

353   Alox15-/- macrophages as compared to WT was higher, suggesting a less efficient trapping (figure

354   7f). It has previously been shown that the decreased motility of Hpb larvae trapped by macrophages

355   can be reversed by Arginase-1 blockade. We first assessed Arginase-1 activity after Hpb and

356   immune serum incubation in Alox15-/- macrophages, and as in our Nb L3 and IL-4 assays,

357   Arginase-1 activity was markedly enhanced in KO macrophages (figure 7g). We further

358   determined that despite a notable difference in the drivers of macrophage polarization (antibodies

359   versus IL-4), Arginase-1 blockade was not able to further increase motility in Alox15-/-

360   macrophages (figure 7f).

361   To further generalize our findings, we took advantage of a recently published single cell RNA

362   sequencing dataset comparing BALB/c versus B6 pleural immune cells in their response against

363   the filarial pathogen *Litomosoides sigmodontis [39]*. The authors did show that in BALB/c

364   susceptible mice, the presence of Type 1 cytokines prevent incoming monocytes to fully

365   differentiate in tissue resident cells and to M2 shift. Interestingly, we found that Alox15 expression

366   was enriched in tissue macrophages in resistant C57BL/6 mice after infection, but not in

367   transitional hybrid M1/M2 macrophages in susceptible BALB/c mice (Figure S4b). Furthermore,

368   like in the case of infection with Nb and Hpb, Arg1 and Rtnla expression were similar between the

369   two macrophage populations.

370   Altogether, these observations show that Alox15 is a crucial enzyme involved in macrophage M2

371   commitment, thus affecting anti-helminth immunity.

372

373   **PPARδ activation can overcome Alox15 deficiency in helminth mediated trapping/killing**

374   Alox15 is a lipid metabolizing enzyme, with a broad role in the production and metabolism of lipid

375   mediators important in health and diseases [19]. Recently, Alox15 has been proposed to be a key

376   metabolizing enzyme in T regulatory cell differentiation and regulatory phenotypes [40]. In

377   absence of Alox15, Tregs had low FOXP3 expression and a high glycolytic profile.

378   Supplementation with resolvins, lipid mediators downstream of DPA, EPA or DHA, rescued the

379   altered T regulatory phenotype. Due to the parallels between our findings, we reasoned that Alox15

380   deficiency in M(IL-4) could be rescued by lipid supplementation.

381   To identify such lipids of interest, we performed lipidomic analysis of Hpb-infected intestines 4

382   days after secondary infection in WT and in Alox15-/- mice. Larval products of Hpb have

383   previously been shown to trigger a broad anti-inflammatory eicosanoid shift after primary

384   infection by suppressing the 5-lipoxygenase pathway, and inducing the cyclooxygenase (COX)

385   pathway [41]. In secondary infection, arachidonic acid as well as linoleic acid were found in a

386   similar quantity in WT and Alox15-/- animals (figure 8a). 12 and 15-HETE, two downstream

387   products of Arachidonic acid were significantly decreased in Alox15-/- intestine as compared to

388   WT counterparts. Similarly 17-HDHA, downstream of DHA was also reduced in Alox15-/- tissue.

389   Although not significant, a similar trend could be observed for 9 and 13-HODEs downstream of

390   Linoleic acid. We found no significant difference between genotypes in any other eicosanoids

391   tested or in RvD1 (figure 8a).

392   Omega-6 PUFAs are the most abundant polyenoic fatty acids in mammalian cells and are thus

393   major lipoxygenase (LOX) substrates. We thus focused first on arachidonic acid and linoleic acid

394   metabolism. Using the Hpb trapping assay, we performed rescue experiments by supplementing

395   with 9-HODE, 13-HODE and 15-HETE the most common downstream mediator products of

396   Alox15. However, none of those reversed the increase Hpb motility observed in co-culture assay

397   with Alox15 deficient macrophages (Figure S5a).

398   Given we had also observed a decrease in Omega-3 (n-3) PUFA downstream products of Alox15,

399   we further considered if those could be involved in our helminth-specific phenotype. It has recently

400   been shown that n-3 DPA supplementation can enhance macrophage efferocytosis and

401   phagocytosis [42]. We thus assessed if n-3 DPA supplementation could rescue the absence of

402   trapping/killing observed in Alox15 deficient macrophages. Indeed, n-3 DPA supplementation

403   rescued the trapping of Hpb larvae by Alox15-/- macrophages (Figure 8b). To confirm, this

404   phenotype reversal was not specific to Hpb trapping or BMDM, we performed an *ex vivo* binding

405   assay with IL-4 polarized lung macrophages and Nb larvae. Similarly, DPA was able to rescue the

406   binding of Nb larvae by Alox-15 deficient macrophages (Fig S4B).

407   Given Omega-3 PUFAs and downstream metabolites are ligands, or partial-ligands, of peroxisome

408   proliferator-activated receptors (PPAR), we next used an agonists of PPAR-γ and PPAR-δ,

409   Rosiglitazone and GW501516 respectively as another method to validate that enhancing lipid

410   metabolism could reverse the Alox15-/- phenotype. Interestingly, both PPAR agonists rescued the

411 macrophage larvicidal activity against Hpb larvae (Fig S4C). GW501516, the PPAR-δ agonist led

412 to a significant reversal in the impaired ability of Alox15-/- macrophages to reduce larval motility,

413 similar to the trend observed with exogenous DPA (Figure 8c).

414 To further confirm that Alox15 downstream lipid metabolites control anti-helminth activity

415 through PPAR mediated control of glycolysis, we performed Seahorse XF analysis of glycolysis

416 and OXPHOS after rescuing Alox15-/- M(IL-4) with PPAR-δ stimulation. As expected both

417 glycolysis (Figure 8d) and OXPHOS (Fig S4D) normalized to the level obtained for WT.

418 Altogether our results show that Alox15 metabolism of DPA activates PPAR-δ that in turn controls

419 glycolysis activation to ensure full M2 commitment.

420

Discussion

422 Macrophages are central to anti-helminth immunity in the vast majority of mouse models but are

423 largely unstudied in human helminthiasis. In rodents, macrophages require a so-called 'alternative'

424 or "M2" activation mediated by type 2 cytokines or antibodies [4-6, 29, 34]. This M2 signature is

425 also enhanced by collectins and stress signals [25, 30]. However, macrophage M2 polarization

426 differs between mouse and human, at least in terms of hallmark genes. With the long-term goal of

427 elucidating anti-helminth role of macrophage in humans, we investigated Alox15, an arachidonate

428 lipoxygenase that is a hallmark of human macrophage alternative activation [12, 19]. Upon genetic

429 deletion of Alox15, we found that macrophages cannot efficiently trap and kill hookworm larvae

430 in mice, nor could they repair tissue damage. Interestingly, hallmark genes of alternatively

431 activated macrophages were not compromised, begging the question as to why there was a loss of

432 function. We further found that Alox15-/- macrophages activated with IL-4 displayed a hybrid

433 phenotype of classical and alternative activation. This was associated with an uncontrolled switch

434 to glycolysis. We finally show that to ensure a 'pure' M2 commitment, Alox15 derived metabolites

435 of DPA are required to activate PPAR-δ, which keeps glycolysis in check.

436 For several decades, hallmark M2 genes have been used as a readout of alternative activation. Our

437 study demonstrates that upregulation of such genes was not sufficient for functional activation; *i.e.*

438 trapping helminth parasites or repairing tissue damaged by parasite's migration. Notably,

439 Arginase-1 has previously been proposed to participate in macrophage-mediated protection against

440   helminths as both a marker and enzymatic effector molecule [4-6, 29]. Our observation that

441   Arginase 1 activity did not functionally correlate with anti-helminth activity is in line with recent

442   findings showing that macrophage-specific STAT6 activation is dispensable for trapping *H.*

443   *polygyrus* in an arginase-independent manner [9]. Instead, Westermann and colleagues propose

444   that intestinal epithelial cells make an important contribution to the formation of intestinal

445   granulomas in a STAT6 dependent manner. However, the authors show that macrophage STAT6

446   expression is still required for protection against *N. brasiliensis* in line with our previous findings

447   [4]. Here, we found that Alox15 expression in macrophages was required for both *H. polygyrus*

448   and Nb trapping *in vitro*. We further confirmed *in vivo* that macrophage deficiency solely in

449   macrophage is sufficient to cause a loss of protection.

450   For both Nb and Hpb, macrophages binding to the larvae was compromised by Alox15 deficiency,

451   suggesting that parasite recognition might be affected by Alox15 deficiency. However, comparing

452   Arginase-1 blockade (by BEC) with Alox15 genetic deficiency did not lead to any common genes

453   downregulated. It is important to note here that this transcriptomic analysis was performed after

454   24 hours of IL-4 stimulation, but Alox15 expression is known to peak at 48 hours, therefore it is

455   possible we simply missed the optimal window to assess this response [43].

456   *N. brasiliensis* infection in mice typically gives a rapid, 'pure' Th2 response. This textbook anti-

457   helminth immunity is distinct from that observed outside the laboratory, as human or wild animal

458   helminthiasis is characterized by a 'modified type 2' response thought to be a hybrid of Th2/Th1/

459   Tregs [44, 45]. Although there are discrepancies in the literature, chronic human hookworm

460   infection has been associated with a mixed cytokine response; IFNg, TNFa, and IL-10 are elevated

461   in the serum in addition to IL-5 [46-48]. Recently, CyToF of helminth-exposed patients has

462   deepened our understanding of the immune response in humans and confirmed this hybrid

463   response is due to ILC2s, and CD4+, CD8+, and γδ T cells [46]. To date, we could not find any

464   reports of mixed polarization of macrophages in helminth infected individuals, however this is

465   likely due to the fact that peripheral responses are studied in the context of human helminth

466   infection. In future, flow cytometry of, for example, sputum samples from infected patients could

467   give insights into macrophage polarization. We speculate that in this mixed cytokine environment,

468   macrophages might not commit to a purely 'alternative' phenotype, and instead develop a hybrid

469   M1/M2 commitment as recently shown for sequential IL-4/LPS stimulation [49]. Given the central

470   role of M2 macrophages in protection against reinfection in rodent helminth models, such a defect

471   in M2 polarization could explain why hookworm-infected individuals are highly susceptible to re-

472   infection for life. In line with this idea, Finlay et al. recently compared two mouse genotypes with

473   different susceptibility to filarial infection and reported that in the presence of Type 1 cytokines,

474   tissue resident macrophages do not properly adopt the M2 phenotype, and instead display lower

475   OXPHOS and heightened phagocytosis. [39] Interestingly, despite an overall decrease in an IL-4-

476   associated gene signature, the authors report that the hallmark M2 genes were not strongly

477   affected, similar to our model. By reanalyzing the single cell sequencing data published by Finlay

478   and colleagues, we have further shown that Alox15 expression, but not Arginase 1, was correlated

479   with parasite clearance and efficient M2 polarization, highlighting that Alox15 is likely to be a

480   generic anti-helminth feature of macrophage polarization.

481

482   As highly plastic cells, the polarisation of macrophage activation has been described as a

483   continuum with 'classical' and 'alternative' states at either end. While comparisons of *in vivo* and

484   *in vitro* datasets have begun to challenge the simplicity of this model [33, 50], the terms are still

485   widely used. It has been proposed in recent years that classically activated macrophages enhance

486   their glycolysis to meet their energetic need, while alternatively activated macrophages use the

487   more energy efficient oxidative phosphorylation. Yet there is some conflict over the requirement

488   for glycolysis in alternative activation [33, 50], which is thought to be due, in part, to the use of

489   the inhibitor 2-DG to block glycolysis; 2-DG appears to have off target effects on OXPHOS

490   activity. There is reason to suspect that intact glycolysis is required for efficient anti-helminth

491   immunity. For example, inhibiting glucose utilization by intraperitoneal injection of 2-DG during

492   *H. polygyrus* infection perturbs M2 polarisation, significantly reducing expression of RELMa [51].

493   Furthermore, it has been noted that alveolar macrophages are not protective against the lung phase

494   of *N. brasiliensis* infection as they are hyporesponsive to IL-4 due to the glucose-restricted

495   environment of the alveolar niche [32].

496   While M1 polarization clearly requires metabolic reprogramming, M2 polarization may be more

497   subtle. In our own study, we noted that OXPHOS activity was not different between basal 'M0'

498   and IL-4 activated 'M2' bone marrow-derived macrophages. Here, we argue that glycolysis needs

499   to be kept in check to obtain a functional M2 commitment. Failing in that control results in the

500 development of a hybrid M1/M2 signature which lacks anti-helminth activity, but retains M1

501 functions, such as anti-*Leishmania* control. This suggests that alternative effector functions are

502 more tightly regulated than classical effector functions. In line with our work, a hybrid M1/M2

503 signature has recently been reported after sequential exposure of BMDM to IL-4 and LPS *in vitro*,

504 with a metabolic profile matching the one we described for Alox15-/- M(IL-4), *i.e.* a heightened

505 glycolysis at the same time as a heightened OXPHOS[49]. The authors then prove that the pro-

506 inflammatory genes expressed by hybrid M1/M2 macrophages require HIF-1α stabilization as in

507 the case of 'classical' polarization. Whether this also occurs in the absence of Alox15-/- should be

508 further investigated. Other hybrid M1/M2 macrophage phenotypes have recently been reported in

509 response to IL-33 stimulation which elicits the co-expression at the protein and mRNA level of

510 alternative markers (Arg1, Retnla, Chil3, Alox15…) as well as pro-inflammatory markers (IL-6,

511 IL-1b) [52]. Interestingly, IL-33-induced hybrid polarization did not display enhanced glycolysis

512 but rather full integrity of the TCA cycle. IL-33 is very strongly released in the lungs after Nb

513 infection and given we observed stronger transcriptional differences *in vivo* that *in vitro* between

514 WT and Alox15-/- macrophages, it could be the case that Alox15 is also important to the fine

515 tuning of IL-33 activation of macrophages.

516 Despite a staggering number of publications on Alox15, its role in cellular metabolism has not

517 been well-studied to date. Namgaladze et al. first established the possible involvement of Alox15

518 in cellular immunometabolism in 2015 [53]. Indeed, the authors showed that AMPK inhibition

519 blocked Alox15 upregulation after IL-4 stimulation, but did not further characterize the activation

520 profile of said macrophages. Instead, they investigated the role of AMPK and Alox15 in the IL-4

521 priming effect prior to LPS activation. In this context, they could show that Alox15 deficiency

522 decreased the pro-inflammatory signature of IL-4 primed macrophages. Treatment with 12- or 15-

523 HETE instead of IL-4 could similarly potentiate pro-inflammatory cytokine production in

524 macrophages. In our model, 12- and 15-HETE supplementation was not sufficient to restore the

525 anti-helminth activity of Alox15-/- M(IL-4). We have unfortunately not assessed cytokines

526 production after this supplementation. However, n-3 DPA supplementation, another lipid substrate

527 for Alox15, was able to restore a 'pure' M2 commitment in Alox15-/- M(IL-4), both functionally

528 and metabolically. A current limitation of our study is that we have not identified the responsible

529 downstream metabolite(s) of DPA.

530 Interestingly a similar finding has been reported in regulatory T cells[40], where Alox15

531 deficiency has been shown to dampen Treg activation and cause upregulation of pro-inflammatory

532 factors. Supplementation with resolvins –downstream products of Alox15 activity on DPA/DHA

533 – was shown to rescue Treg activation. Of note, the functional relevance of resolvins is a highly

534 debated topic in the field due to their production in very low quantity and the associated challenge

535 of detecting them with current technology. Using metabolomics, the authors reported heightened

536 glycolysis and TCA in Alox15-/- Tregs. Together with our results, this suggests that the

537 SPMs/Alox15 pathway might be crucial as a 'confirmation signal' to allow the development of a

538 pro-repair, anti-helminth M2 commitment. Failure to deliver this secondary signal may then push

539 the immune cell towards a pro-inflammatory phenotype as a 'fail-safe' or 'default' pathway.

540

541 **Methods**

542 **Reagents**

543 The following reagents were used in various assays : IL-4 10 ng/mL (Peprotech), LPS 10 ng/ml

544 (Peprotech), IFNg : 10 ng/mL (Peprotech) and were reconstituted in PBS.

545 BEC 1 uM (Sigma), Rosiglitazone 0.1, 0.5, 1uM (PPAR-γ agonist, Sigma), GW501516 0.1, 1,

546 5uM (PPAR-δ agonist, Sigma), n-3 Docosapetaenoic acid sodium salt DPA 100uM (Cayman

547 Chemical) 15-HETE (Cayman Chemical), 13-HODE (Cayman Chemical), 9-HODE (Cayman

548 Chemical) were reconstituted in DMSO (Sigma).

549

550 **Mice**

551 C57BL/6J (WT) mice were obtained from Charles River Laboratories (Germany) or from Animal

552 Resources Center (Australia). All mice were maintained under specific pathogen-free (SPF)

553 conditions at École Polytechnique Fédérale de Lausanne (EPFL), Switzerland or by the Monash

554 Intensive Care Unit Facility at Monash University, AMREP campus Melbourne, Australia or by

555 the Animal Facility, Swiss TPH, Switzerland. All mice were age and sex-matched and used

556 between 8-14 weeks of age. Littermates of the same sex were randomly assigned to experimental

557 groups. Mice were maintained at 3-5 animal per cage and ad libidum access to water and food. All

558 animal experiments were approved by the Service de la consommation et des affaires vétérinaires

559 (1066 Épalinges, Canton of Vaud, Switzerland) with the authorization number VD 3001, or by the

560 AEC committee of the Alfred campus, Melbourne Australia with authorization number

561 E/1846/2018/M or by BL/543/2022.

562

Preparation and Isolation of *N. brasiliensis* Larvae

564 Nb was maintained by monthly passage in Lewis rats. Infective larvae (L3) were prepared from 2

565 week old rat fecal cultures as previously described (Camberis et al., 2003). 550L3 or 250 L3 were

566 delivered by subcutaneous injection in 100 μL of sterile PBS to the scruff of the neck.

567 Viable larvae were recovered from tissue (lung or gut) by baerman at 37 °C for at least 2 h as

568 previously reported (my method paper). Viable worms follow a thermal gradient and migrate out

569 of the bag to collect at the bottom for counting. Larvae present in the large airways were harvested

570 by bronchoalveolar lavage, with 3×1 ml of PBS, followed by filtering on 40 um gause. For larvae

571 count and red blood cell count, the 3ml of wash were pooled together. Larvae were manually

572 counted under brightfield on a stereomicroscope. Red blood cells were counted with a

573 haemocytometer, after centrifugation of the BALF and resuspended in 1 ml to account for the

574 difference of BALF volume harvested in each mouse. D0 marks the day of infection. If not

575 explicitly mentioned, the time between primary and reinfection was 30 days.

576 For adoptive transfer, 1.7-2 million cells (stimulated for 24 hrs with IL-4) were administered

577 intranasally in 50 μl of PBS, the evening prior to infection with 550L3.

578

Preparation and Isolation of *H. polygyrus bakeri* Larvae

580 The standard Hpb infective stage-three larvae (L3) were generated in the laboratory based on

581 published protocols [54]. 200 L3 were administered per os as previously described [6]. Viable

582 worm burden were obtained by baerman as previously described [55]. Granulomas were

583 enumerated by manual counting of the small intestinal contents under a dissecting microscope. D0

584 marks the day of infection. If not explicitly mentioned, the time between primary and reinfection

585 was 30 days.

586

Leishmania mexicana maintenance and infection

588 Transgenic *L. mexicana* stably expressing the fluorescent protein TurboRFP (L.
589 mexicanaTurboRFP) were maintained in promastigote stage at 27°C in RPMI media pH 7.4
590 supplemented with 10% FCS with biweekly passaging. Only cultures <20 passages since isolation
591 from infected murine tissue were used to generate amastigotes for infections. Amastigotes were
592 generated by incubating stationary phase promastigotes in RPMI media pH 5.5 supplemented with
593 20% FCS for 4 days at 33°C 5% CO2.

594

Macrophage generation

596 For bone marrow-derived macrophages, marrow was flushed from the femur and tibia of C57BL/6
597 mice and passed through cell strainers (70 µm) in PBS. The cells (10^6 mL^{-1}) were cultured in 30%
598 M-CSF (supernatant of L929 cell culture) supplemented medium (RPMI (Gibco), 10% FCS
599 (Gibco), penicillin/streptomycin) for 7 days as described previously [34]. Macrophages were
600 harvested between day 7 and 10 of culture for experiments.

601 For lung macrophages, mice were either used naïve or infected with 250 or 550 L3 subcutaneously.
602 The lungs were washed by bronchoalveolar lavage with 3 mL of PBS and then digested in media
603 (DMEM (Gibco), 2 mg mL^{-1} collagenase (Sigma), DNase 12.5 U mL^{-1} (Roche, Sigma-Aldrich,
604 Merck & Cie, Schaffhausen, Switzerland)) at 37°C on an orbital shaker for 45 min. The cells were
605 passed through a cell strainer (70 µm) and seeded (2.5×10^5) directly in a flat-bottom 96-well plate.
606 Non-adherent cells were washed away the following day and adherent macrophages were cultured
607 in complete DMEM (10% FCS, 1% penicillin/streptomycin) for 2 days before co-culture with
608 larvae.

Larval binding assay

Nb assay: macrophages were polarized or not with recombinant IL-4 (10 ng mL^{-1}) and various inhibitors or agonists (see reagents) for 24 hours. 0.1×10^6 cells were then co-cultured with 100 third-stage *N. brasiliensis* larvae (Nb L3) in 96-well plates, and the number of larvae with >10 cells attached to their surface was manually counted by light microscopy after 4 days of co-culture [56], and expressed as a percentage of total larvae per well.

Hpb assay: 0.1×10^6 BMDM were co-cultured with 100 third-stage *H. polygyrus bakeri* (Hpb) in presence of immune serum. Inhibitors, supplements or agonists were provided 24 hours prior to adding the larvae. All co-cultures were performed at 37℃, 5% CO_2, for 24 h. The percentage of motile larvae attacked by macrophages were then quantified using a stereo microscope.

Larval viability assessment

After the co-culture, Sytox green was added (1:100, Life technologies, Cat#S7020) to the wells and viability of the larvae was assessed using fluorescent microscopy. Larvae were considered dead, or to have impaired viability, when staining positive for the dye, and expressed as a percentage of total larvae per well.

Leishmania/macrophage co-culture assays

BMDM infection with *L. mexicanaTurboRFP* and subsequent flow cytometric analysis were performed as described previously [57]. Briefly, BMDMs were seeded into non-treated 96-well plates at 110,000 cells/well. Following overnight incubation at 33℃, BMDMs were co-incubated with *L. mexicanaTurboRFP* amastigotes at a low (0.5:1) or high (3:1) multiplicity of infection at 33℃ 5% CO2 for the indicated period. At the indicated time point, infected macrophages were gently detached from plates and single cell suspensions were stained with a fixable viability dye, anti-F4/80 and anti-CD11b, and analyzed by flow cytometry. Dead cells and extracellular parasites were excluded prior to gating of infected macrophages (SSChiFSChiF4/80+CD11b+TurboRFP-H+) and uninfected macrophages (SSChiFSChiF4/80+CD11b+TurboRFP-H-). Data was analyzed using FlowJo software where infected macrophages are expressed as the percentage of gated

637 viable, single macrophages. The TurboRFP geometric mean fluorescence intensity (gMFI) of

638 infected macrophages minus that of uninfected macrophages was used as an indicator of average

639 parasitic burden. Parasitic index, the product of the percent infection and parasitic burden, was

640 used as a more general readout of infection.

RNA isolation and RT-qPCR

642 RNA of 1×106 cells was extracted with a TriPure (Sigma-Aldrich), and reverse transcribed using

643 FIREScript RT cDNA synthesis Kit Solis Biodyne (Lucerna 06-15-00200) for qPCR analysis.

644 qPCR was performed using PowerUp SYBR green Applied Biosystems (Thermofisher A25741)

645 on an Bio-Rad CFX96 touch Real-Time PCR detection system. Data analysis was performed with

646 CFX Maestro, and expression was normalized according to expression of the housekeeping gene

647 GAPDH.

Multiplex PCR

649 Custom oligonucleotide primers and probes (Table 5) were designed using National Center for

650 Biotechnology Information (Bethesda, Md) primer blast software and were purchased from

651 Microsynth (Balgach, Switzerland). Amplification was carried out using iQ Multiplex Powermix

652 and a CFX96 Real-Time detection system using forward and reverse primers at a concentration of

653 $10\mu M$ and probes at a concentration of $50\mu M$. Absolute quantification was performed using the

654 CFX Manager software 2.1 (all from Bio-Rad) based on values obtained with a set of purified

655 amplicons used as standards.

656 Table 5. oligonucleotide primers and probes for multiplex PCR analysis

Oligonucleotide name	NCBI reference sequence	5' label	Sequence
Retnla/Fizz1_forward	NM_020509.3	-	5'-TTGCCAATCCAGCTAACTATCCCT -3'
Retnla/Fizz1_reverse		-	5'-AGCACACCCAGTAGCAGTCA -3'
Retnla/Fizz1_probe		TX Red	5'-ACAGATGGGCCTCCTGCCCTGCTGGGA-3'
Arg1_forward	NM_007482.3	-	5'-CCTGCTGGGAAGGAAGAAAAGG-3'
Arg1_reverse		-	5'-TCTCTGTAAGATAGGCCTCCCA-3'
Arg1_probe		FAM	5'-TTCACCCCGGCGACCGGCACCCC-3'
Chil3/YM1_forward	NM_009892.3	-	5'-CAAGTTGAAGGCTCAGTGGCTC-3'
Chil3/YM1_reverse		-	5'-TGTCAGAGGGAAATGTCTCTGGT-3'

Chil3/YM1_probe		Cy5	5'-GGAGGTGCCGTGGTCTGGCCCCTGG-3'
MRC1_forward	NM_008625.2	-	5'-TCTGGATTGGACTCAACAGTCT-3'
MRC1_reverse		-	5'-CTCTGATGATGGACTTCCTGGT-3'
MRC1_probe		HEX	5'-ACGCAGTGGTTGGCAGTGGGCTGGAGG-3'
FN1_forward	NM_010233.2	-	5'-CAGCAAGCCACAGTTTCTGATA-3'
FN1_reverse		-	5'-TCTGTAATAGCGCACAGAGACG-3'
FN1_probe		TX Red	5'-TGCCTCCACCCCCACCAGCCTGCTCA-3'
TIMP1_forward	NM_001044384.1	-	5'-GCCCTTCGCATGGACATTTATT-3'
TIMP1_reverse		-	5'-CATGGTATCTGCTCTGGTGTGT-3'
TIMP1_probe		FAM	5'-TCCACTGTGCAGCCCCTGCCGCCA-3'
MMP7_forward	NM_001319986.1	-	5'-CTCTAGGTCATGCCTTCGCA-3'
MMP7_reverse		-	5'-AAGTTCACTCCTGCGTCCTCA-3'
MMP7_probe		Cy5	5'-CCTGGGCCAGGCCTAGGCGGAGA-3'
MMP9_forward	NM_013599.4	-	5'-CCTGGCTCTCCTGGCTTTC-3'
MMP9_reverse		-	5'-ACAAGTATGCCTCTGCCAGC-3'
MMP9_probe		HEX	5'-TGCCCCTTACCAGCGCCAGCCGACTTT-3'
HPRT1_forward	NM_013556.2	-	5'-AGAGCGTTGGGCTTACCTCA-3'
HPRT1_reverse		-	5'-TGGTTCATCATCGCTAATCACGAC-3'
HPRT1_probe		Cy5.5	5'-TTTTGCCGCGAGCCGACCGGTCC-3'

657 The primers and probes specific for Retnla/FIZZ1, ARG1, CHIL3/YM1, MRC1; and FN1,

658 TIMP1, MMP7, and MMP9; were collectively used in multiplex-1, and -2 respectively. The

659 primers and probe specific for HPRT1, our reference gene, were added into each multiplex. *Cy*,

660 Cyanine; *FAM*, fluorescein; *HEX*, hexachloro-fluorescein; *Tx Red*, Texas Red.

661

BMDM transcriptomics

663 Fastq files were processed using the Laxy tool [58] using the RNAsik pipeline [59] using STAR

664 aligner [60] with Mus musculus GRCm38. Reads were quantified using featureCounts [61]

665 producing the raw genes count matrix and various quality control metrics, summarised in MultiQC

666 report [62]. The gene count matrix was analysed with Degust [63], a web tool which performs

667 differential expression analysis using limma voom normalisation producing counts per million

668 (CPM) library size normalisation and trimmed mean of M values (TMM) normalisation for RNA

669 composition, and also several quality plots such as classical multidimensional scaling [MDS] and

670 MA plots. Samples were batched corrected to account for known variation across replicates. This

671 was done within Degust by adding a covariate to the linear model for each sequencing batch which

672 reduced the noise and improved the power of the test. Differentially expressed genes were defined

673 as those showing a >2-fold (log2FC 1) change in expression with a false-discovery rate (FDR) of

674 0.05.

675

676 **Single cell sequencing**

677 Lungs were minced and then digested in media (DMEM (Gibco), 2 mg mL−1 collagenase (Sigma),

678 DNase 12.5 U mL−1 (Roche, SigmaAldrich, Switzerland)) at 37°C on an orbital shaker for 45 min

679 at 105 rpm. Lungs were then passed through a 70µm cell strainer with syringe plungers. Red blood

680 cell lysis was performed (Merck, 11814389001). Whole transcriptome analyses of FACS sorted

681 CD45+ cells were performed using the BD Rhapsody Single Cell Analysis System (BD,

682 Biosciences). Cells were stained with Zombie Aqua live/dead (Biolegend) and Fc block (2.4G2,

683 BioXCell, BE0307) according to maufacturer's instructions. Prior to FACS staining, cells were

684 labelled with sample tags (633793 BD Mouse Single-Cell Multiplexing Kit) according to the

685 manufacturer's protocol. As the CD45 sample tag clone and FACS antibody clone were the same

686 (30-F11), sample tagging was performed in the presence of a 1:1 (w/w) quanitity of anti-CD45

687 FACS antibody. In brief, for each condition, 10^6 cells were resuspended in staining buffer (1%

688 BSA, 1% EDTA in PBS) and incubated with the respective Sample Tag:anti-CD45 BUV395

689 cocktails for 20 min on ice. Cells were then transferred to a 5-ml polystyrene tube, washed twice

690 with 2 ml staining buffer and centrifuged at 400g for 5 min. Samples were stained in a FACS

691 antibody cocktail mix for 20 mins on ice: CD19-APCe780 (1D3, ebioscience, 47-0193-80), Gr-1-

692 PE (RB6-8C5, Biolegend, 108408), SiglecF-PE-CF594 (E50-2440, BD, 562757), Ter-119-Biotin-

693 SA-PECy5 (Biolegend, 116204), CD11c-Pecy7 (HL3, BD, 564079), CD3e-BUV737 (145-2C11,

694 BD, 564618), CD11b-PacBlue (M1/70, Biolegend, 101224), CD4-BV711 (RM4-5, eBioscience,

695 14-0042-83),CD8-BV786(H35-17.2, BD, 740952). Cells were washed and resuspended in 1 ml

696 staining buffer for counting. Next, an equal number of cells from 4 barcoded samples per group

697 were pooled and the mixture was centrifuged at 400g for 5 min. The BD Rhapsody cartridge was

698 loaded with 40,000 cells. Single cells were isolated with the BD Rhapsody Express Single-Cell

699 Analysis System according to the manufacturer's recommendations (BD Biosciences). cDNA

700 libraries were prepared using the BD Rhapsody Whole Transcriptome Analysis Amplification Kit

701 (633801 BD Biosciences) following the BD Rhapsody System mRNA Whole Transcriptome

702 Analysis (WTA) and Sample Tag Library Preparation Protocol (BD Biosciences). The final

703 libraries were quantified using a Qubit Fluorometer with the Qubit dsDNA HS Kit (Q32851

704 Thermo Fisher Scientific). Library size distribution was measured with the Agilent high-sensitivity

705 D5000 assay on a TapeStation 4200 system (5067-5592 Agilent Technologies). Sequencing was

706 performed in paired-end mode (2×75 cycles) on a NovaSeq 6000 with NovaSeq 6000 SP Reagent

707 Kit chemistry.

708

Single cell sequencing analysis

710 Gene quantification was generated with STARsolo (STAR-2.7.10a, [64]) and aligned to a

711 GENCODE Version M29 reference [65] with sample tags added for de-multiplexing purposes.

712 Parameters were in accordance with DB Rhapsody (version 1) with default settings. Subsequently,

713 the resulting filtered matrix underwent quality control assessments and analytical evaluations

714 within the R environment (version 4.3.2, [66]), utilizing various R packages such as SoupX

715 (version 1.6.2, [67]) for the removal of ambient mRNAs, scater (version 1.30.1, [68]) to identify

716 outlier metrics and Seurat (version 5.0.1, [69]). No other cell filtering criteria were applied

717 regarding total number of UMIs, unique expression genes, or mitochondrial gene proportion.

718 However, genes with cell counts less than 3 were excluded. Seurat's demultiplexing function was

719 employed to eliminate doublets and ambiguous cells. Additionally, Seurat's SCTransform was

720 applied using the 'glmGamPoi' method, followed by RunPCA, RunUMAP, FindNeighbors and

721 FindClusters for clustering analysis. Default parameters were utilized, except for employing 40

722 dimensions of input features and proceeding with a resolution of 2 for cluster analysis. Manual

723 annotations were conducted by referencing markers from various published sources [70-76].

724 UMAP figures were customized using ggplot2 (version 3.4.4, 14) [77].

725

Sample preparation for LC-MS/MS

727 For intestinal tissue culture, the intestine was removed, extensively flushed with cold PBS. The

728 intestine was isolated, cut longitudinally and placed separately in 100 mm Petri dishes with PBS

729 containing 10 µg/ml Gentamicin, 100 U/ml Penicillin and 100 µg/ml Streptomycin (all from

730 GIBCO). Opened cut intestines were gently scraped to remove mucus, washed 3 times and

731   transferred into a new Petri dish. The anterior 4 cm of the intestine (duodenum) were cut into 1–2

732   mm pieces and transferred to a 24-well plate with 2 ml/well of RPMI media (PAA Laboratories)

733   containing 10% heat inactivated FCS, 10 µg/ml Gentamicin, 100 U/ml Penicillin and 100 µg/ml

734   Streptomycin (all from GIBCO). 24-well plates were incubated over night at 37°C before

735   supernatants were harvested and analyzed by LC-MS/MS.

736   Samples were prepared as triplicates in medium/MeOH (1:1) or PBS/MeOH (1:1) with an analyte

737   concentration of 0.1, 1, or 10 ng/mL (10× higher concentrations for PUFAs). Automated solid

738   phase extractions were performed with a Microlab STAR robot (Hamilton, Bonaduz, Switzerland).

739   Prior to extraction, all samples were diluted with H_2O to a MeOH content of 15% and 10 μL of IS

740   stock solution was added. Samples were extracted using Strata-X 96-well plates (30 mg,

741   Phenomenex, Aschaffenburg, Germany) and eluted with MeOH. Samples were evaporated to

742   dryness under N_2 stream and redissolved in 100 μL MeOH/H_2O (1:1).

743

744   **LC-MS/MS lipid mediator analysis**

745   Chromatographic separation of eicosanoids was achieved with a 1260 Series HPLC (Agilent,

746   Waldbronn, Germany) using a Kinetex C18 reversed phase column (2.6 μm, 100×2.1 mm,

747   Phenomenex) with a SecurityGuard Ultra Cartridge C18 (Phenomenex) precolumn. The Sciex

748   QTRAP 5500 mass spectrometer (Sciex, Darmstadt, Germany), equipped with a Turbo-V^{TM} ion

749   source, was operated in negative ionization mode. Identification of metabolites was achieved via

750   retention time and scheduled multiple reaction monitoring (sMRM). Unique Q1/Q3 transitions

751   were selected for each analyte by using single analyte injections and comparison with the literature.

752   Analytes with identical MRM transitions were differentiated by retention time as described in [18]

753   **Flow cytometry**

754   BMDM were polarized or not with recombinant IL-4 (10 ng mL^{-1}, peprotech) for 24 hours. The

755   next day, cells were detached with cold PBS and a cell scraper. Isolated cells were resuspended in

756   FACS buffer, and Fc-receptors were blocked (2.4G2) before staining with monoclonal antibodies

757   before collection on a Fortessa flow cytometer (BD). Fluorochrome-conjugated antibodies to the

758   following cell surface molecules were used: CD45-AF700 (30-F11, 1:100, BD Biosciences

759   Pharmingen), F4/80-APCeF780 (BM8, 1:100, Ebiosciences), Arginase-APC (1:100, Abcam), Ki-

760   67-PE (SolA15, 1:10, Ebiosciences). Cell suspensions were stained with LIVE/DEAD fixable

761   aqua dead cell Stain kit (Invitrogen) when fixation was required for intracellular staining. Analysis

762   was performed with the FlowJo software (Treestar).

763

764   **Arginase-1 activity assay**

765   Macrophage arginase-1 activity was determined according to previously published methods [6].

766   Briefly, 300000 adherent macrophages (48 well plate) were lysed and conversion of L-arginine

767   was quantified indirectly by measuring urea production with a QuantiChrom Urea Assay

768   (BioAssay Systems, Hayward, CA).

769

770   **Griess assay**

771   Culture media from L. mexicanaTurboRFP infection assays was harvested by centrifuging to

772   remove cells and retaining supernatant. 50 uL supernatant was first incubated at room temperature

773   for 7 min with 50 uL 0.1% sulfanilamide in phosphoric acid prior to addition of 50 uL N-1-

774   napthylethylenediamine dihydrochloride (NEDD) and a further 7 min incubation. Plates were then

775   analyzed by plate reader at 540 nm. Sample nitrite concentration was determined by a nitrite

776   standard dilution series.

777

778   **Fluorescence imaging**

779   BMDM were grown on 8 chambers ibidi slides, fixed in 2% PFA. Prior to staining, cells were

780   permeabilized in PBS, 0.5% triton X100 (Sigma) and blocked in 5% PBS, BSA (Sigma).

781   stained with DAPI and anti-Alox15 antibody (1:100, Abb244205, Abcam).

782   Granulomas were identified on paraffin sections by light microscopy and serial sections were used

783   for immunofluorescence staining for Arginase-1-AF568 (1:800) and F4/80-AF647 (BM8, 1:300,

784   Ebiosciences) and DAPI (Sigma). Stained tissue sections were imaged with an inverted point

785   scanning confocal microscope (Zeiss LSM 710) with a Plan-Apochromat (63×/1.4 NA or 40×/1.3

786   NA) objective .

787   Alox15 or Arginase intensity was measured in Fiji. To control for differences in background

788   fluorescence between experiments and antibody/dye batches, the contrast was adjusted to

789   minimize autofluorescence and a minimum brightness threshold was set such that only positive

790   staining could be visualized. The same contrast and threshold values were applied to all images

791   taken across all treatment groups within a single experiment using Fiji [78].

792

793

794   **Seahorse flux analysis**

795   BMDM were polarized or not with recombinant IL-4 (10 ng mL^{-1}, peprotech) for 24 hours and

796   with LPS (10 ng/ml, Sigma) for 8 hours. The next day, cells were detached with cold PBS and a

797   cell scraper. Isolated macrophages from individual mice or a pool of 2-3 mice were plated at 50

798   000 cells per well in 96 well plate (100 ul) or at 150 000 cells per well in a 24 well plate (450 ul)

799   in XF media and allowed to adhere for 30 min at 37C, 5%C02. The cells were then transferred for

800   30 min to a 37C incubator without C02 just prior to analysis. ECAR and OCR were measured in

801   XF media under basal conditions, in response to 25 mM glucose, 1.5 μM oligomycin, 1.5 μM

802   FCCP, 1mM Sodium Pyruvate, 0.5 μM Antimycin A, 0.5 μM Rotenone (Sigma) using a 96- or 24-

803   well extracellular flux analyzer XFe-96 and XFe-24 (Seahorse Bioscience) as previously described

804   [79].

805

Data analysis

807   All data were analyzed using GraphPad Prism 8.2 (GraphPad Software, La Jolla, CA, USA) or R

808   3.4.3.21. For LC-MS/MS analysis, all samples were normalized to their RNA content. Data were

809   analyzed using Wilcoxon, Friedman, or Kruskal-Wallis test with respective post hoc test as

810   appropriate. Significant differences were defined at $P < 0.05$.

References

812   1.   Diemert, D.J., et al., *Lessons along the Critical Path: Developing Vaccines against Human Helminths.* Trends Parasitol, 2018. **34**(9): p. 747-758.

814   2.   Coakley, G. and N.L. Harris, *Interactions between macrophages and helminths.* Parasite Immunol, 2020. **42**(7): p. e12717.

816   3.   Lechner, A., S. Bohnacker, and J. Esser-von Bieren, *Macrophage regulation & function in helminth infection.* Semin Immunol, 2021. **53**: p. 101526.

818   4.   Bouchery, T., et al., *ILC2s and T cells cooperate to ensure maintenance of M2 macrophages for lung immunity against hookworms.* Nat Commun, 2015. **6**: p. 6970.

820   5.   Chen, F., et al., *Helminth resistance is mediated by differential activation of recruited monocyte-derived alveolar macrophages and arginine depletion.* Cell Rep, 2022. **38**(2): p. 110215.

822   6.   Esser-von Bieren, J., et al., *Antibodies trap tissue migrating helminth larvae and prevent tissue damage by driving IL-4Ralpha-independent alternative differentiation of macrophages.* PLoS Pathog, 2013. **9**(11): p. e1003771.

825   7.   Goldman-Pinkovich, A., et al., *An Arginine Deprivation Response Pathway Is Induced in Leishmania during Macrophage Invasion.* PLoS Pathog, 2016. **12**(4): p. e1005494.

827   8.   Muxel, S.M., et al., *Arginine and Polyamines Fate in Leishmania Infection.* Front Microbiol, 2017. **8**: p. 2682.

829   9.   Westermann, S., et al., *Th2-dependent STAT6-regulated genes in intestinal epithelial cells mediate larval trapping during secondary Heligmosomoides polygyrus bakeri infection.* PLoS Pathog, 2023. **19**(4): p. e1011296.

832   10. Thomas, A.C. and J.T. Mattila, *"Of mice and men": arginine metabolism in macrophages.* Front Immunol, 2014. **5**: p. 479.

834   11. Ackermann, J.A., et al., *The double-edged role of 12/15-lipoxygenase during inflammation and immunity.* Biochim Biophys Acta Mol Cell Biol Lipids, 2017. **1862**(4): p. 371-381.

836   12. Czimmerer, Z., et al., *Identification of novel markers of alternative activation and potential endogenous PPARgamma ligand production mechanisms in human IL-4 stimulated differentiating macrophages.* Immunobiology, 2012. **217**(12): p. 1301-14.

839   13. Gundra, U.M., et al., *Alternatively activated macrophages derived from monocytes and tissue macrophages are phenotypically and functionally distinct.* Blood, 2014. **123**(20): p. e110-22.

841   14. Schif-Zuck, S., et al., *Saturated-efferocytosis generates pro-resolving CD11b low macrophages: modulation by resolvins and glucocorticoids.* Eur J Immunol, 2011. **41**(2): p. 366-79.

843   15. Snodgrass, R.G., et al., *A Novel Function for 15-Lipoxygenases in Cholesterol Homeostasis and CCL17 Production in Human Macrophages.* Front Immunol, 2018. **9**: p. 1906.

845   16. Uderhardt, S., et al., *12/15-lipoxygenase orchestrates the clearance of apoptotic cells and maintains immunologic tolerance.* Immunity, 2012. **36**(5): p. 834-46.

847 17.   Werz, O., et al., *Human macrophages differentially produce specific resolvin or leukotriene signals*
848   *that depend on bacterial pathogenicity.* Nat Commun, 2018. **9**(1): p. 59.
849 18.   Henkel, F.D.R., et al., *House dust mite drives proinflammatory eicosanoid reprogramming and*
850   *macrophage effector functions.* Allergy, 2019. **74**(6): p. 1090-1101.
851 19.   Snodgrass, R.G. and B. Brune, *Regulation and Functions of 15-Lipoxygenases in Human*
852   *Macrophages.* Front Pharmacol, 2019. **10**: p. 719.
853 20.   Bleich, D., et al., *Resistance to type 1 diabetes induction in 12-lipoxygenase knockout mice.* J Clin
854   Invest, 1999. **103**(10): p. 1431-6.
855 21.   Cyrus, T., et al., *Absence of 12/15-lipoxygenase expression decreases lipid peroxidation and*
856   *atherogenesis in apolipoprotein e-deficient mice.* Circulation, 2001. **103**(18): p. 2277-82.
857 22.   Cyrus, T., et al., *Disruption of the 12/15-lipoxygenase gene diminishes atherosclerosis in apo E-*
858   *deficient mice.* J Clin Invest, 1999. **103**(11): p. 1597-604.
859 23.   Pernet, E., et al., *Neonatal imprinting of alveolar macrophages via neutrophil-derived 12-HETE.*
860   Nature, 2023. **614**(7948): p. 530-538.
861 24.   Huang, J.T., et al., *Interleukin-4-dependent production of PPAR-gamma ligands in macrophages by*
862   *12/15-lipoxygenase.* Nature, 1999. **400**(6742): p. 378-82.
863 25.   Bosurgi, L., et al., *Macrophage function in tissue repair and remodeling requires IL-4 or IL-13 with*
864   *apoptotic cells.* Science, 2017. **356**(6342): p. 1072-1076.
865 26.   Entwistle, L.J., et al., *Epithelial-Cell-Derived Phospholipase A(2) Group 1B Is an Endogenous*
866   *Anthelmintic.* Cell Host Microbe, 2017. **22**(4): p. 484-493 e5.
867 27.   Thomas, G.D., et al., *The biology of nematode- and IL4Ralpha-dependent murine macrophage*
868   *polarization in vivo as defined by RNA-Seq and targeted lipidomics.* Blood, 2012. **120**(25): p. e93-
869   e104.
870 28.   Green-Mitchell, S.M., et al., *Deletion of 12/15-lipoxygenase alters macrophage and islet function*
871   *in NOD-Alox15(null) mice, leading to protection against type 1 diabetes development.* PLoS One,
872   2013. **8**(2): p. e56763.
873 29.   Chen, F., et al., *An essential role for TH2-type responses in limiting acute tissue damage during*
874   *experimental helminth infection.* Nat Med, 2012. **18**(2): p. 260-6.
875 30.   Minutti, C.M., et al., *Local amplifiers of IL-4Ralpha-mediated macrophage activation promote*
876   *repair in lung and liver.* Science, 2017. **356**(6342): p. 1076-1080.
877 31.   Gordon, S. and A. Pluddemann, *Tissue macrophages: heterogeneity and functions.* BMC Biol, 2017.
878   **15**(1): p. 53.
879 32.   Svedberg, F.R., et al., *The lung environment controls alveolar macrophage metabolism and*
880   *responsiveness in type 2 inflammation.* Nat Immunol, 2019. **20**(5): p. 571-580.
881 33.   Van den Bossche, J., L.A. O'Neill, and D. Menon, *Macrophage Immunometabolism: Where Are We*
882   *(Going)?* Trends Immunol, 2017. **38**(6): p. 395-406.
883 34.   Bouchery, T., et al., *beta-Glucan receptors on IL-4 activated macrophages are required for*
884   *hookworm larvae recognition and trapping.* Immunol Cell Biol, 2022. **100**(4): p. 223-234.
885 35.   Pessenda, G. and J.S. da Silva, *Arginase and its mechanisms in Leishmania persistence.* Parasite
886   Immunol, 2020. **42**(7): p. e12722.
887 36.   Schleicher, U., et al., *TNF-Mediated Restriction of Arginase 1 Expression in Myeloid Cells Triggers*
888   *Type 2 NO Synthase Activity at the Site of Infection.* Cell Rep, 2016. **15**(5): p. 1062-1075.
889 37.   Wanasen, N. and L. Soong, *L-arginine metabolism and its impact on host immunity against*
890   *Leishmania infection.* Immunol Res, 2008. **41**(1): p. 15-25.
891 38.   Tomiotto-Pellissier, F., et al., *Macrophage Polarization in Leishmaniasis: Broadening Horizons.*
892   Front Immunol, 2018. **9**: p. 2529.
893 39.   Finlay, C.M., et al., *T helper 2 cells control monocyte to tissue-resident macrophage differentiation*
894   *during nematode infection of the pleural cavity.* Immunity, 2023. **56**(5): p. 1064-1081 e10.

40. Marques, R.M., et al., *Loss of 15-lipoxygenase disrupts T(reg) differentiation altering their pro-resolving functions.* Cell Death Differ, 2021. **28**(11): p. 3140-3160.

41. de Los Reyes Jimenez, M., et al., *An anti-inflammatory eicosanoid switch mediates the suppression of type-2 inflammation by helminth larval products.* Sci Transl Med, 2020. **12**(540).

42. Pistorius, K., et al., *PD(n-3 DPA) Pathway Regulates Human Monocyte Differentiation and Macrophage Function.* Cell Chem Biol, 2018. **25**(6): p. 749-760 e9.

43. Han, H., et al., *Interleukin-4-mediated 15-lipoxygenase-1 trans-activation requires UTX recruitment and H3K27me3 demethylation at the promoter in A549 cells.* PLoS One, 2014. **9**(1): p. e85085.

44. Diaz, A. and J.E. Allen, *Mapping immune response profiles: the emerging scenario from helminth immunology.* Eur J Immunol, 2007. **37**(12): p. 3319-26.

45. Loke, P., S.C. Lee, and O.O. Oyesola, *Effects of helminths on the human immune response and the microbiome.* Mucosal Immunol, 2022. **15**(6): p. 1224-1233.

46. de Ruiter, K., et al., *Helminth infections drive heterogeneity in human type 2 and regulatory cells.* Sci Transl Med, 2020. **12**(524).

47. Quinnell, R.J., et al., *Immune responses in human necatoriasis: association between interleukin-5 responses and resistance to reinfection.* J Infect Dis, 2004. **190**(3): p. 430-8.

48. Pit, D.S., et al., *Parasite-specific antibody and cellular immune responses in human infected with Necator americanus and Oesophagostomum bifurcum.* Parasitol Res, 2001. **87**(9): p. 722-9.

49. Dang, B., et al., *The glycolysis/HIF-1alpha axis defines the inflammatory role of IL-4-primed macrophages.* Cell Rep, 2023. **42**(5): p. 112471.

50. Kieler, M., M. Hofmann, and G. Schabbauer, *More than just protein building blocks: how amino acids and related metabolic pathways fuel macrophage polarization.* FEBS J, 2021. **288**(12): p. 3694-3714.

51. Huang, S.C., et al., *Metabolic Reprogramming Mediated by the mTORC2-IRF4 Signaling Axis Is Essential for Macrophage Alternative Activation.* Immunity, 2016. **45**(4): p. 817-830.

52. Faas, M., et al., *IL-33-induced metabolic reprogramming controls the differentiation of alternatively activated macrophages and the resolution of inflammation.* Immunity, 2021. **54**(11): p. 2531-2546 e5.

53. Namgaladze, D., et al., *AMP-activated protein kinase suppresses arachidonate 15-lipoxygenase expression in interleukin 4-polarized human macrophages.* J Biol Chem, 2015. **290**(40): p. 24484-94.

54. Moyat, M., et al., *Microbial regulation of intestinal motility provides resistance against helminth infection.* Mucosal Immunol, 2022. **15**(6): p. 1283-1295.

55. Bouchery, T., et al., *The Study of Host Immune Responses Elicited by the Model Murine Hookworms Nippostrongylus brasiliensis and Heligmosomoides polygyrus.* Curr Protoc Mouse Biol, 2017. **7**(4): p. 236-286.

56. Chen, F., et al., *Neutrophils prime a long-lived effector macrophage phenotype that mediates accelerated helminth expulsion.* Nat Immunol, 2014. **15**(10): p. 938-46.

57. McGowan, E.N.S., et al., *Tetraspanin CD82 restrains phagocyte migration but supports macrophage activation.* iScience, 2022. **25**(7): p. 104520.

58. Powell, A.P.a.D., *Laxy Genomics Pipelines*. 2020, Zenodo.

59. Tsyganov, K., et al., *RNAsik: A Pipeline for complete and reproducible RNA-seq analysis that runs anywhere with speed and ease.* Journal of Open Source Software, 2018. **3**(28): p. 583.

60. Dobin, A., et al., *STAR: ultrafast universal RNA-seq aligner.* Bioinformatics, 2013. **29**(1): p. 15-21.

61. Liao, Y., G.K. Smyth, and W. Shi, *featureCounts: an efficient general purpose program for assigning sequence reads to genomic features.* Bioinformatics, 2014. **30**(7): p. 923-30.

62. Ewels, P., et al., *MultiQC: summarize analysis results for multiple tools and samples in a single report.* Bioinformatics, 2016. **32**(19): p. 3047-8.

63. Powell, D.R., A. Perry, and M. Milton, *Degust: Interactive Rna-Seq Analysis*. David R. Powell, Andrew Perry, Michael Milton, zenodo.

64. Dobin, A., et al., *STAR: ultrafast universal RNA-seq aligner.* Bioinformatics, 2012. **29**(1): p. 15-21.

65. Frankish, A., et al., *GENCODE reference annotation for the human and mouse genomes.* Nucleic Acids Res, 2019. **47**(D1): p. D766-D773.

66. Team, R.C., *R: A language and environment for statistical computing.* R Foundation for Statistical Computing, 2021. **Vienna**(Austria).

67. Young, M.D. and S. Behjati, *SoupX removes ambient RNA contamination from droplet-based single-cell RNA sequencing data.* Gigascience, 2020. **9**(12).

68. McCarthy, D.J., et al., *Scater: pre-processing, quality control, normalization and visualization of single-cell RNA-seq data in R.* Bioinformatics, 2017. **33**(8): p. 1179-1186.

69. Hao, Y., et al., *Dictionary learning for integrative, multimodal and scalable single-cell analysis.* Nat Biotechnol, 2024. **42**(2): p. 293-304.

70. Aegerter, H., B.N. Lambrecht, and C.V. Jakubzick, *Biology of lung macrophages in health and disease.* Immunity, 2022. **55**(9): p. 1564-1580.

71. Du, Y., et al., *'LungGENS': a web-based tool for mapping single-cell gene expression in the developing lung.* Thorax, 2015. **70**(11): p. 1092-1094.

72. Du, Y., et al., *Lung Gene Expression Analysis (LGEA): an integrative web portal for comprehensive gene expression data analysis in lung development.* Thorax, 2017. **72**(5): p. 481-484.

73. Du, Y., et al., *Lung Gene Expression Analysis Web Portal Version 3: Lung-at-a-Glance.* American Journal of Respiratory Cell and Molecular Biology, 2021. **64**(1): p. 146-149.

74. Hu, X., et al., *Single-cell transcriptomics reveals distinct cell response between acute and chronic pulmonary infection of Pseudomonas aeruginosa.* MedComm (2020), 2022. **3**(4): p. e193.

75. Program, C.S.-C.B., et al., *CZ CELL×GENE Discover: A single-cell data platform for scalable exploration, analysis and modeling of aggregated data.* bioRxiv, 2023: p. 2023.10.30.563174.

76. Travaglini, K.J., et al., *A molecular cell atlas of the human lung from single-cell RNA sequencing.* Nature, 2020. **587**(7835): p. 619-625.

77. Wickham, H., *ggplot2: Elegant Graphics for Data Analysis*. 2016: Springer-Verlag New York.

78. Schindelin, J., et al., *Fiji: an open-source platform for biological-image analysis.* Nat Methods, 2012. **9**(7): p. 676-82.

79. Van den Bossche, J., J. Baardman, and M.P. de Winther, *Metabolic Characterization of Polarized M1 and M2 Bone Marrow-derived Macrophages Using Real-time Extracellular Flux Analysis.* J Vis Exp, 2015(105).

Acknowledgements

989

Author contributions

991   T.B., N.L.H. and J.E. conceived of the idea. T.B., N.L.H., J.E. and R.D. participated in the writing

992   of the paper. R.D., T.B., M.M., C.G., V.B. conducted *in vivo* and *in vitro* experiments and

993   downstream analysis. W.L. performed histology analysis. T.V. and U.N. performed qPCR analysis.

994   H.F. performed lipidomics. C.R. performed sequencing of the single cell. B.A. conducted the

995   analysis of the single cell dataset, both under M.B. supervision. S.A. performed the analysis of the

996   lung RNA sequencing dataset. D.D. complemented the analysis of late Nick Wong at the Monash

997   Bioinformatic platform for the BMDM RNA sequencing dataset. M.E.N.S and B.K performed the

998   work on *Leishmania*. All authors discussed the results and commented on the paper.

Competing interests.

1000   There is no competing interest to declare.

1001

Materials & Correspondence.

1003   Correspondence and material requests should be addressed to tiffany.bouchery@swisstph.ch.

1004

Figure Legends

Figure 1: Alox15 deficiency leads to impaired protection against rodent hookworm, and reduced wound healing in the mouse lung.

1008   **A.** B6 mice were infected with 550 Nb L3s subcutaneously of left untreated (D0). 40 days post

1009   infection, mice were either left untreated (D40) or reinfected subcutaneously with 550 Nb L3s

1010   (D40 +D2) for 2 days. Lungs were harvested and CD45+ cells were isolated and prepared for

single-cell sequencing on the BD Rhapsody platform (n= 4 mice per condition). UMAP visualization of scRNA-seq data of D0 (n=XXX), D40 (n=XXX) and D40+D2 (n=XXX) identifying 20 distinct cell clusters or visualized by treatment conditions. **B**. Normalized expression of *Alox15* transcripts across all cell types and shown by treatment conditions. **C,** Alox15-/- and B6 controls were infected twice with 250 Nb L3. Two days after secondary infection, larvae were collected and enumerated from BALF and baermann of lung tissue. N=5 mice per group, 2 independent experiments **D.** Hemorrhage was assessed 5 days post primary infection in BALF. N=5 mice per group, 2 independent experiments. **E.** Haemorrhage was assessed 2 days after a secondary infection. Representative photographs of lungs from B6 and Alox15-/-. N=5 mice per group, 2 independent experiments **F.** Worm burden 5 days post primary infection in Alox15-/- and B6 mice. N=5 mice per group, 3 independent experiments NS, non-significant (p>0.05); *, p≤0.05; ** p≤0.05; *** p≤0.001

Figure 2: Alox15 expression in macrophages is required for larvicidal activity and tissue repair. *In vitro* and *ex vivo* co-cultures of macrophages and *Nippostrongylus brasiliensis* (Nb) larvae were used to assess the requirement of Alox15 for anti-helminth functions. Murine bone marrow-derived macrophages were grown from C57BL/6/J or ALOX-15$^{-/-}$ mice and polarized with recombinant IL-4 for 24 hours. **A.** 2. 10^6 BMDM (IL-4) cells were intranasally administered to naïve C57BL/6/J mice. The next day, mice were infected with 550 L3 of Nb. Two days after infection, larvae were collected and enumerated from BALF and baermann of lung tissue. N=5 mice per group, 2 independent experiments. **B.** BMDM (IL-4) were co-cultured with 100 third-stage *N. brasiliensis* larvae (Nb L3). The percentage of larvae with more than 10 cells attached was assessed for each genotypes. **C.** Representative brightfield microscopy of IL-4 stimulated BMDM (M(IL-4)) bound to Nb L3 as described in B. **D.** Lungs of uninfected B6 or Alox15$^{-/-}$ mice were digested enzymatically and isolated macrophages used for co-culture assay as in A. (n=2-4 mice, 4 independent experiments). **E.** Viability of larvae from C., was measured using the cell impermeable fluorescent dye, Sytox Green.

1039 **Figure 3: Alox15 deficiency cause a loss of function in M(IL-4) independently of Arginase-1**

1040 **activity**

1041 Murine bone marrow-derived macrophages were grown from C57BL/6/J (B6) or ALOX-15$^{-/-}$ mice

1042 and polarized or not (M0) with recombinant IL-4 (M(IL4)) for 24 hours. A. Gene expression of

1043 hallmark genes associated with M(IL-4) polarization obtained by RT-qPCR and expressed as z-

1044 score. (n=3) **B.** Mean Fluorescence Intensity of Arginase-1 analyzed by flow cytometry. (n=3) **C.**

1045 Arginase-1 activity measured by urea production. (n=3, 2 independent experiments). **D.** BMDM

1046 (IL-4) were co-cultured with 100 third-stage *N. brasiliensis* larvae (Nb L3). The percentage of

1047 larvae with more than 10 cells attached was assessed for each genotypes and conditions. (n=4-6, 2

1048 independent experiments). **E.** Murine bone marrow-derived macrophages were grown from

1049 C57BL/6/J (B6) or LysMcre Arg1 flox mice and polarized with recombinant IL-4 (M(IL4)) for 24

1050 hours. Immunofluorescence against Alox15 was performed and acquired on a confocal

1051 microscope. Intensity of staining was analyzed using Fiji. (n=5) **F.** Metascape pathway enrichment

1052 analysis of genes commonly upregulated in Alox15 deficient and BEC treated M(IL-4) as

1053 compared to untreated B6 M(IL-4). (n=3-4) **G.** Gene expression of hallmark genes associated with

1054 M(IL-4) polarization obtained from RNA sequencing and expressed as z-score. Note that none of

1055 those genes were identified as DEGs (n=3-4).

1056

1057 **Figure 4: Alox15 deficiency enable development of a M1/M2 hybrid after IL-4 polarization**

1058 A. mRNA expression profiles (volcano plots) as determined by RNA-sequencing isolated from

1059 total lung macrophages from B6 or ALOX-15$^{-/-}$ mice 7 days post-infection with Nb L3. Red,

1060 significantly differentially expressed genes with a P value <0.01 (n=4-5, representative of 2

1061 independent experiments). B. Pathway enrichment using Metascape of DE genes upregulated in

1062 ALOX-15$^{-/-}$ lung macrophages. C. Gene expression of hallmark genes associated with

1063 macrophages M1 or M2 polarization obtained from RNA sequencing and expressed as z-score. *

1064 corrected P-value <0.05. D. Pathway enrichment using Metascape of DE genes downregulated in

1065 ALOX-15$^{-/-}$ lung macrophages. E. Pathway enrichment using Metascape of a cluster of DE genes

1066 downregulated in ALOX-15$^{-/-}$ lung macrophages with a strong signature in metabolism.

1067

1068 **Figure 5: Alox15 deficient M1/M2 hybrid have a heightened energetic profile after IL-4**

1069 **stimulation**

1070 Total lung macrophages from B6 or ALOX-15^{-/-} mice 7 days post-infection with Nb L3. A. Gene

1071 expression of hallmark genes associated with the glycoltic pathway obtained from RNA

1072 sequencing and expressed as z-score. B Gene expression of hallmark genes associated with

1073 OXPHOS pathway obtained from RNA sequencing and expressed as z-score. C. OCR and SRC

1074 (Spare respiratory Capacity) of BMDM stimulated or not with IL-4 or LPS from both B6 or

1075 ALOX-15^{-/-} mice at baseline and after sequential treatment (vertical lines) with glucose (Gluc.),

1076 oligomycin (OM), FCCP and Pyruvate, Antimycin-A (AA) and Rotenone (rot) as a combined Mito

1077 and Glycolytic stress test [79]. Data representative of 3-4 independent experiments, n = 5 wells per

1078 conditions, each conditions with 1-3 mice per experiments. D. ECAR and Glycolytic capacity of

1079 BMDM stimulated or not with IL-4 or LPS from both B6 and ALOX-15^{-/-} mice as described in C.

1080 E. BMDM stimulated with IL-4 in normal medium (IL-4), with IL-4 in Seahorse medium in

1081 absence of glucose (IL-4 low glucose) or in Seahorse medium with glucose (IL-4 high glucose)

1082 were co-cultured with 100 third-stage *N. brasiliensis* larvae (Nb L3). The percentage of larvae with

1083 more than 10 cells attached was assessed for each genotypes.

1084

1085 **Figure 6: Alox15 deficiency do not impair macrophage control of *Leishmania major***

1086 **A.** Murine bone marrow-derived macrophages were grown from C57BL/6/J (B6) or ALOX-15^{-/-}

1087 mice and polarized or not (M0) with recombinant IL-4, with IL-13, with a combination of IL-4

1088 and IL-13, with LPS or LPS and IFNg for 24 hours. Then those were co-cultured with 100 third-

1089 stage *N. brasiliensis* larvae (Nb L3). The percentage of larvae with more than 10 cells attached

1090 was assessed for each genotypes. n=3, pool of 1-2 independent experiments. **B.** Parasitic index

1091 relative to control of a low dose of L. Mexicana infection of BMDM grown from C57BL/6/J (B6)

1092 or ALOX-15^{-/-} mice. The proportion of macrophages infected with *L. mexicana-TurboRFP* was

1093 measured 4 h to 144h later by flow cytometry. (n=3, 3 independent experiments) **C.** Nitrite

1094 concentration measure by Griess assay (n=3, 2 independent experiments) **D.** Parastic index as in

1095 B after a high dose of infection (n=3, 3 independent experiments)

1096

Figure 7: Alox15 is required for macrophage mediated protection against *H. polygyrus*

A-D. Alox15-/- and B6 controls were infected twice with 200 Hpb L3. 4 or 14 days after secondary infection, parasites and granulomas were enumerated from the small intestine. N=4-5 mice per group, 2 independent experiments. **E.** Immunofluorescence staining of Arginase and F4/80 in intestinal granulomas surrounding Hpb larvae at 4 days post-reinfection. N= 5-6, Quantification from 8-10 granulomas for each genotypes. **F.** Murine bone marrow-derived macrophages were grown from C57BL/6/J (B6) or ALOX-15$^{-/-}$ mice. Differentiated BMDM were co-cultured with 100 third-stage Hpb larvae in presence of immune serum (IS) and with or without the arginase inhibitor BEC. The percentage of motile larvae was assessed for each genotypes by microscopy. n=3-9 mice, pool of 3 independent experiments. **G**. Arginase-1 activity of BMDM stimulated for 24 hours with IS and 100 Hpb L3 measured by urea production. (n=6, representative of 2 independent experiments).

Figure 8: Heightened glycolysis cause loss of anti-helminth killing in Alox15-/- M2

A. LC-MS/MS analysis of LOX metabolites of Arachidonic acid (AA), of Linoleic acid (LA) and of Docosahexaenoic acid (DHA) in intestinal culture supernatants from Hpb infected mice N=4 per genotype, baseline for B6 N=2. **B&C.** Murine bone marrow-derived macrophages were grown from C57BL/6/J (B6) or ALOX-15$^{-/-}$ mice. Differentiated BMDM were co-cultured with 100 third-stage Hpb larvae in presence of immune serum (IS) and with or without the Docosapentaenoic acid (DPA) or a PPARd agonist. The percentage of motile larvae was assessed for each genotypes by microscopy. N= 3-6 per condition, pool from 3 independent experiments. Of note B&C share some of the DMSO conditions. **D.** Glycolytic capacity of BMDM stimulated as with IL-4 and/or PPARd agonist for 24 hours prior to the assay. Data representative of 3 independent experiments, n = 5 wells per conditions, each conditions with 1-3 mice per experiments.
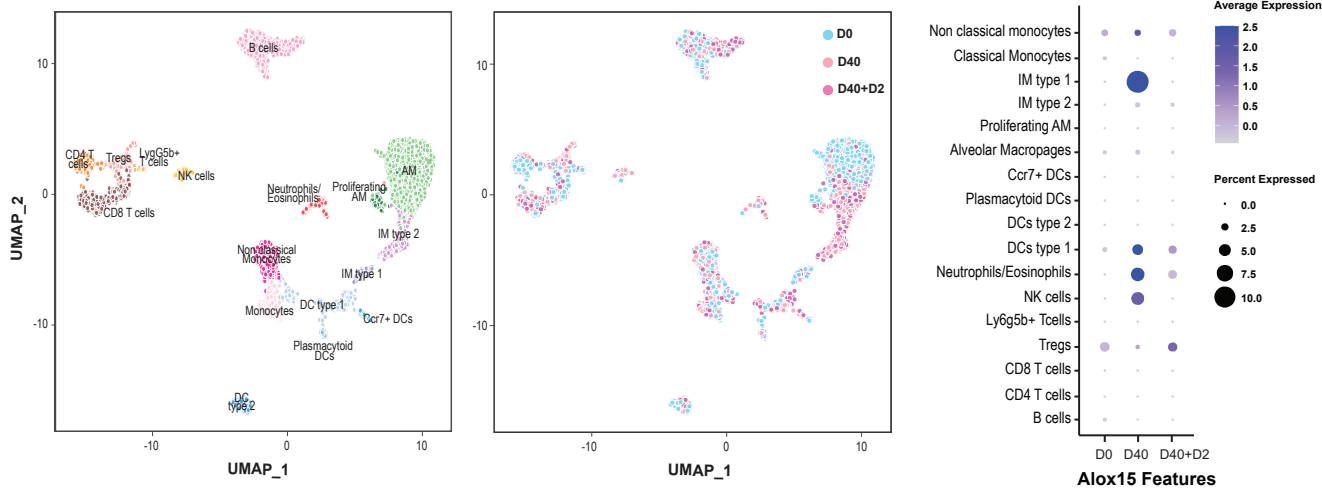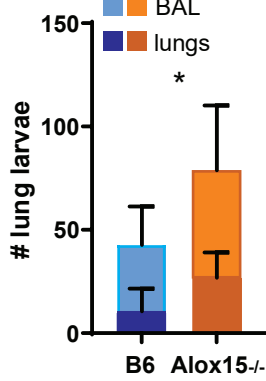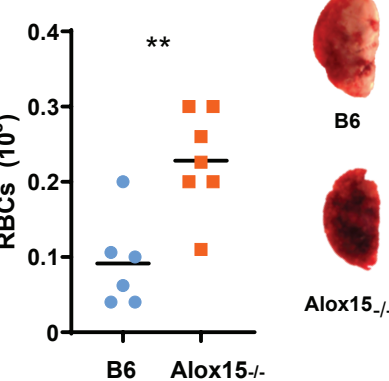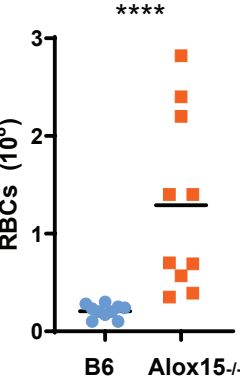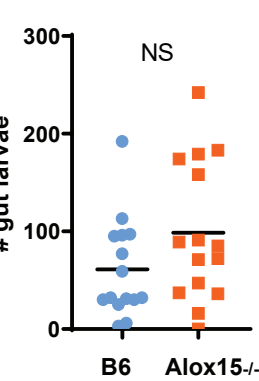
Figure 1: Alox15 deficiency leads to impaired protection against rodent hookworm, and reduced wound healing in the mouse lung.
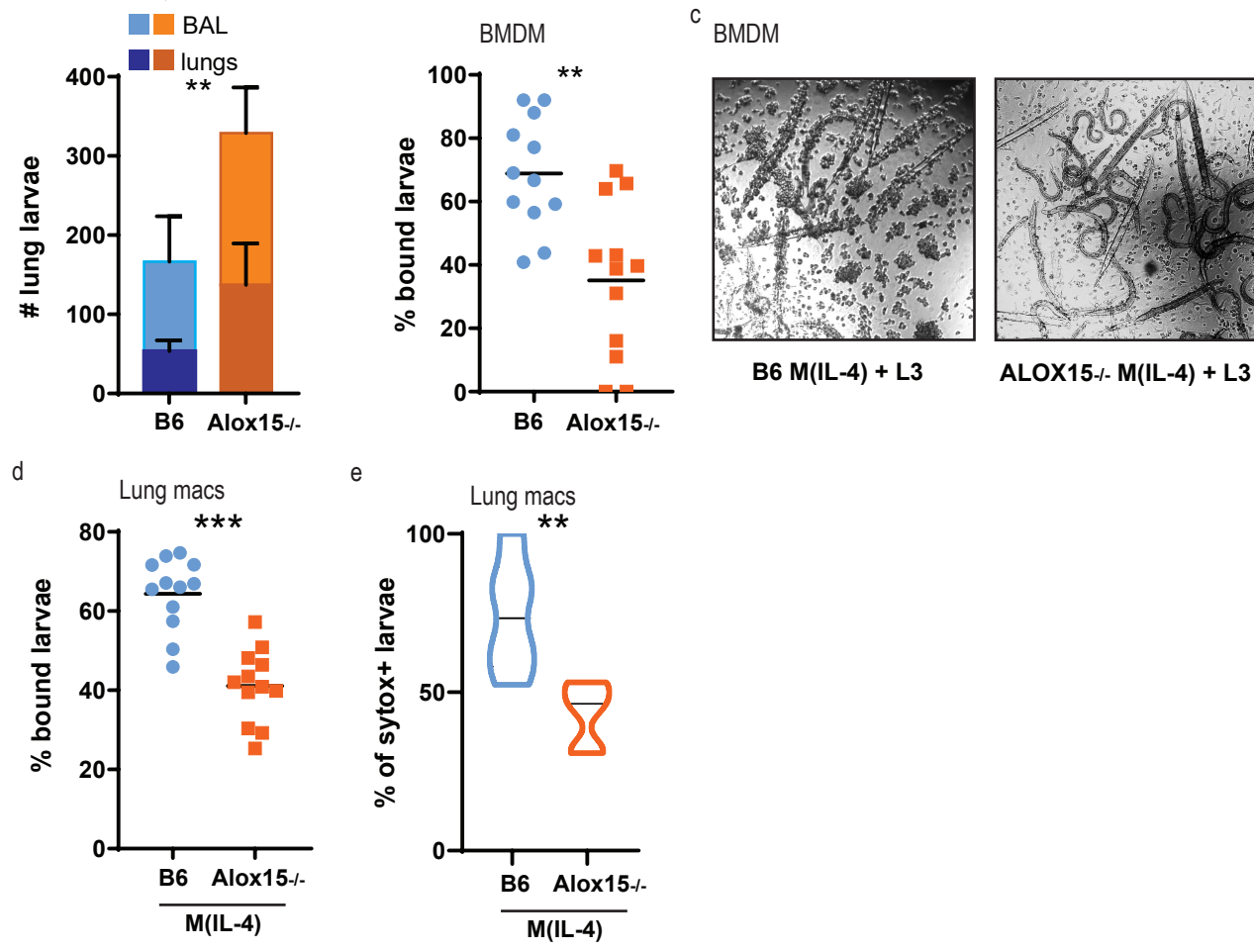
Figure 2: Alox15 expression in macrophages is required for larvicidal activity and tissue repair.
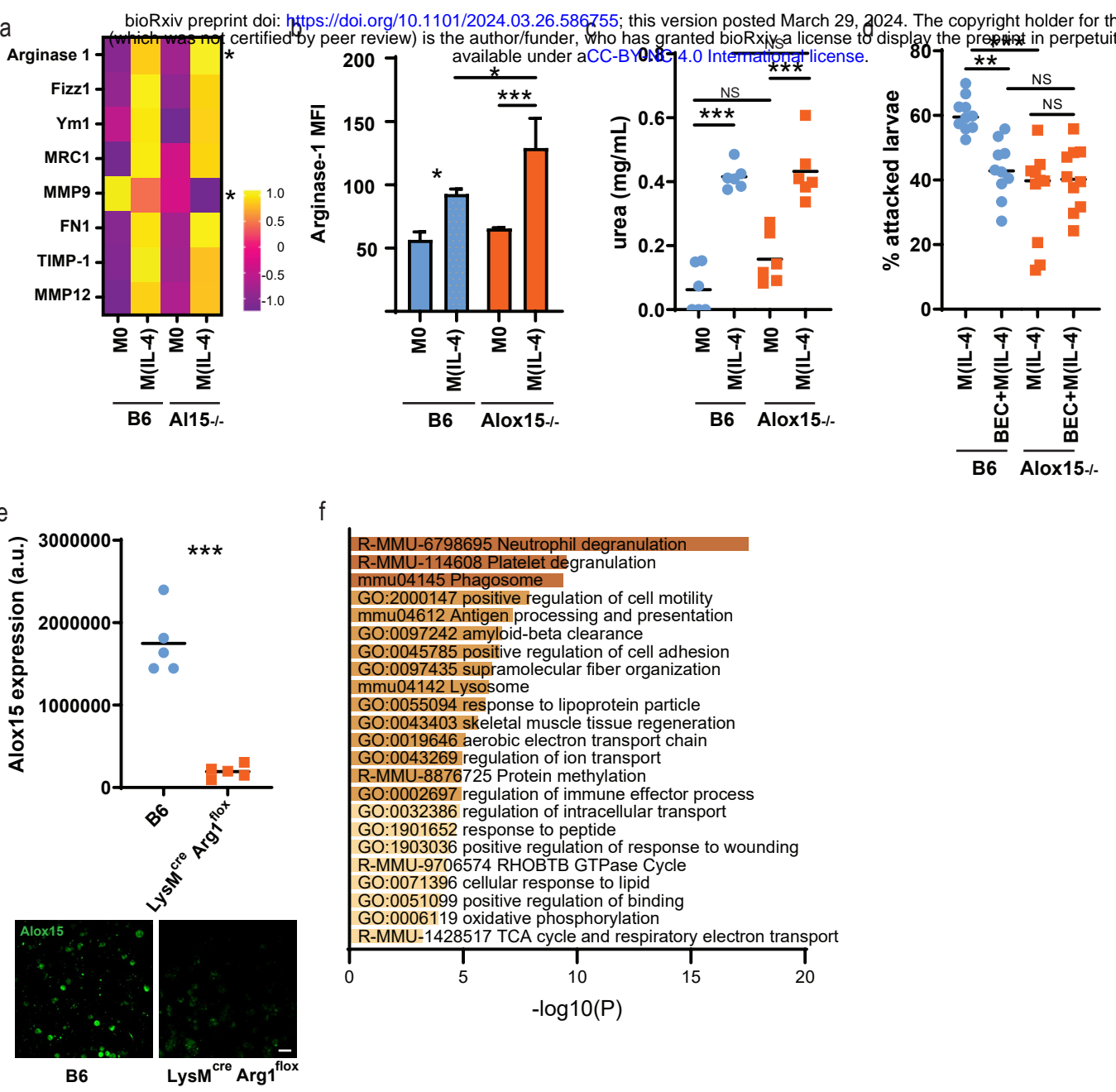
Figure 3: Alox15 deficiency cause a loss of function in M(IL-4) independently of Arginase-1 activity
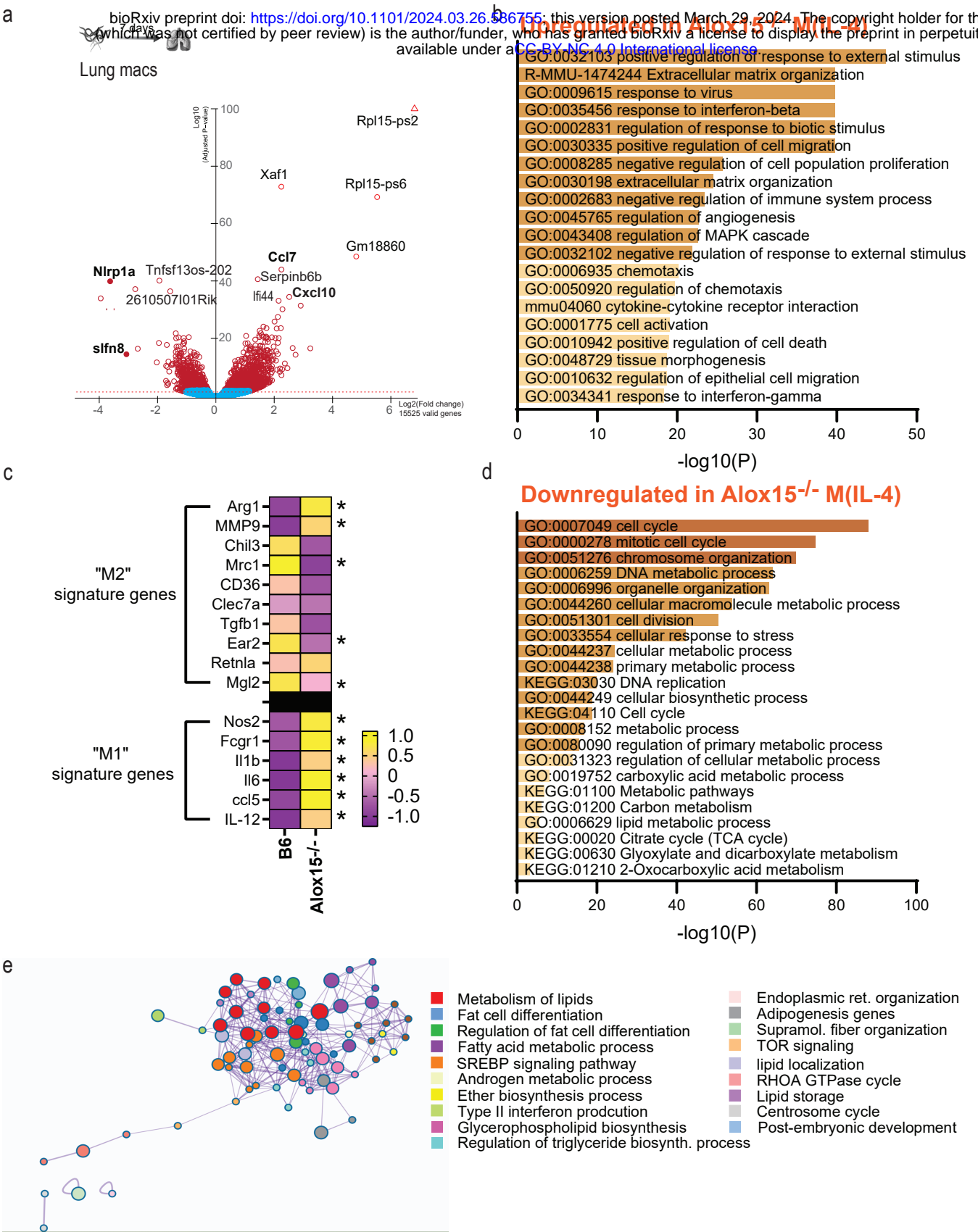
Figure 4: Alox15 deficiency enable development of a M1/M2 hybrid after IL-4 polarization
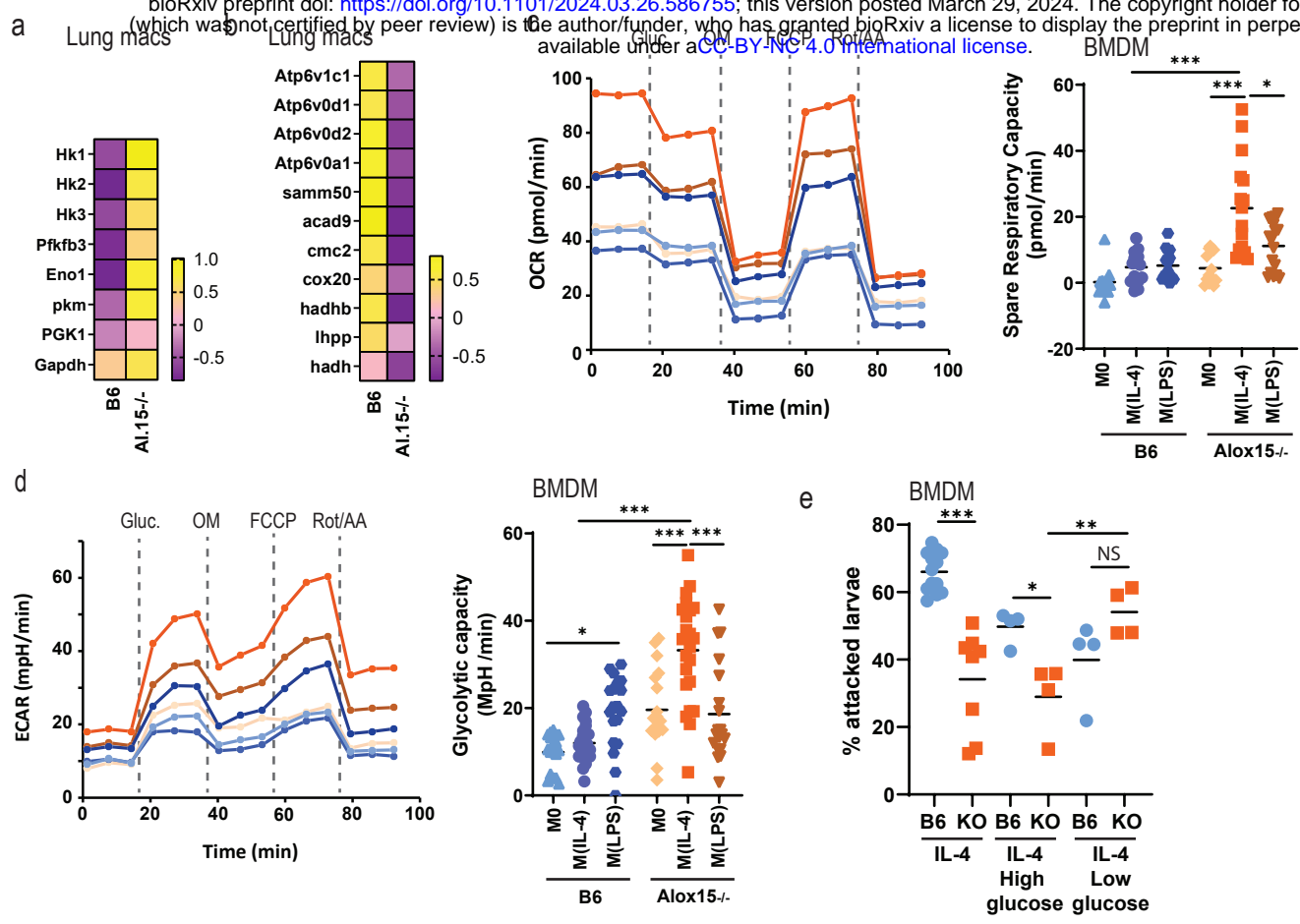
Figure 5: Alox15 deficient M1/M2 hybrid have a heightened energetic profile after IL-4 stimulation

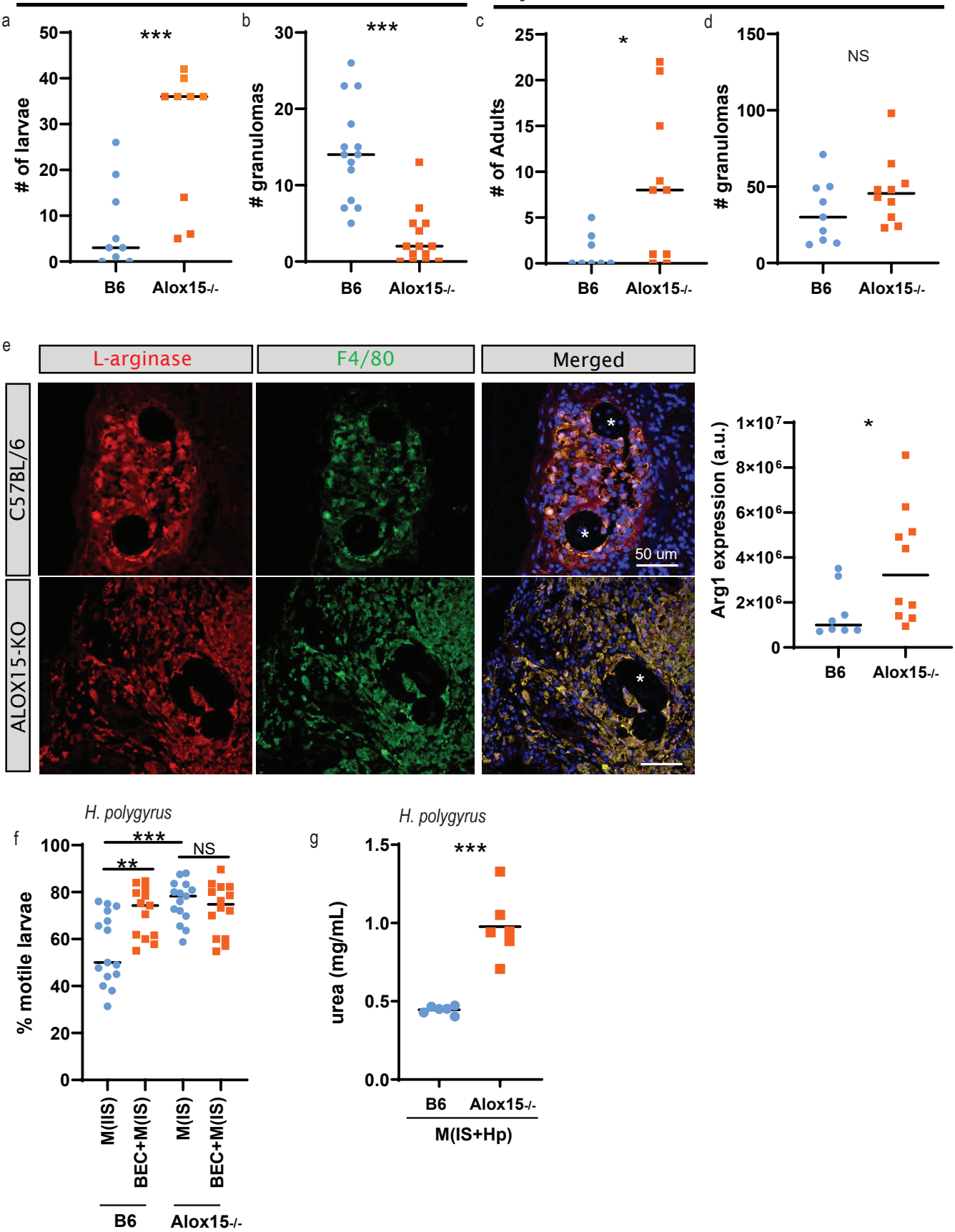Figure 6: Alox15 deficiency do not impair macrophage control of Leishmania major

H. polygyrus

Day 4

Day 14

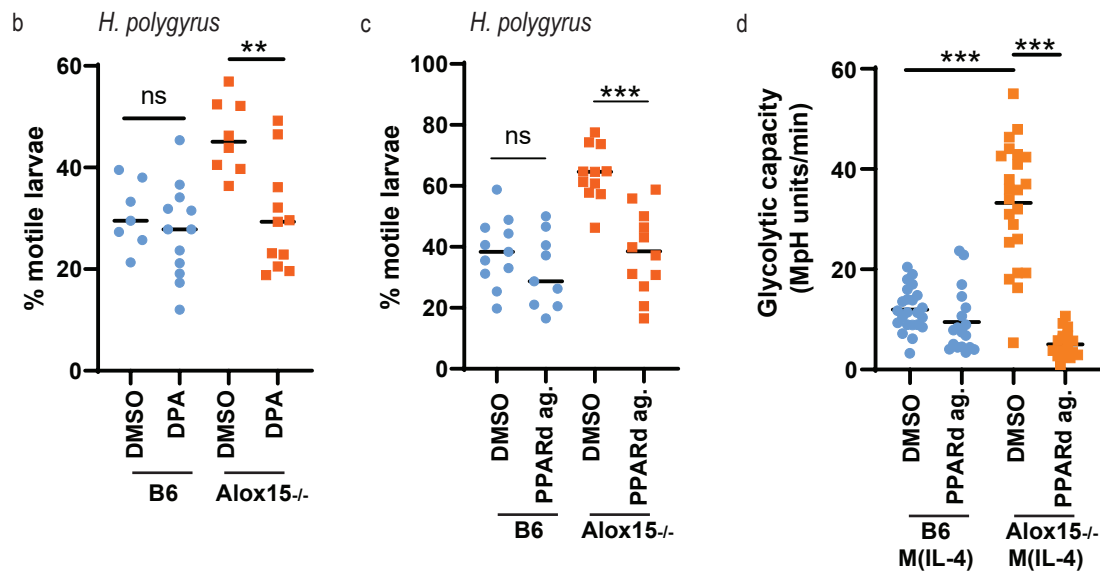Figure 7: Alox15 is required for macrophage mediated protection against H. polygyrus
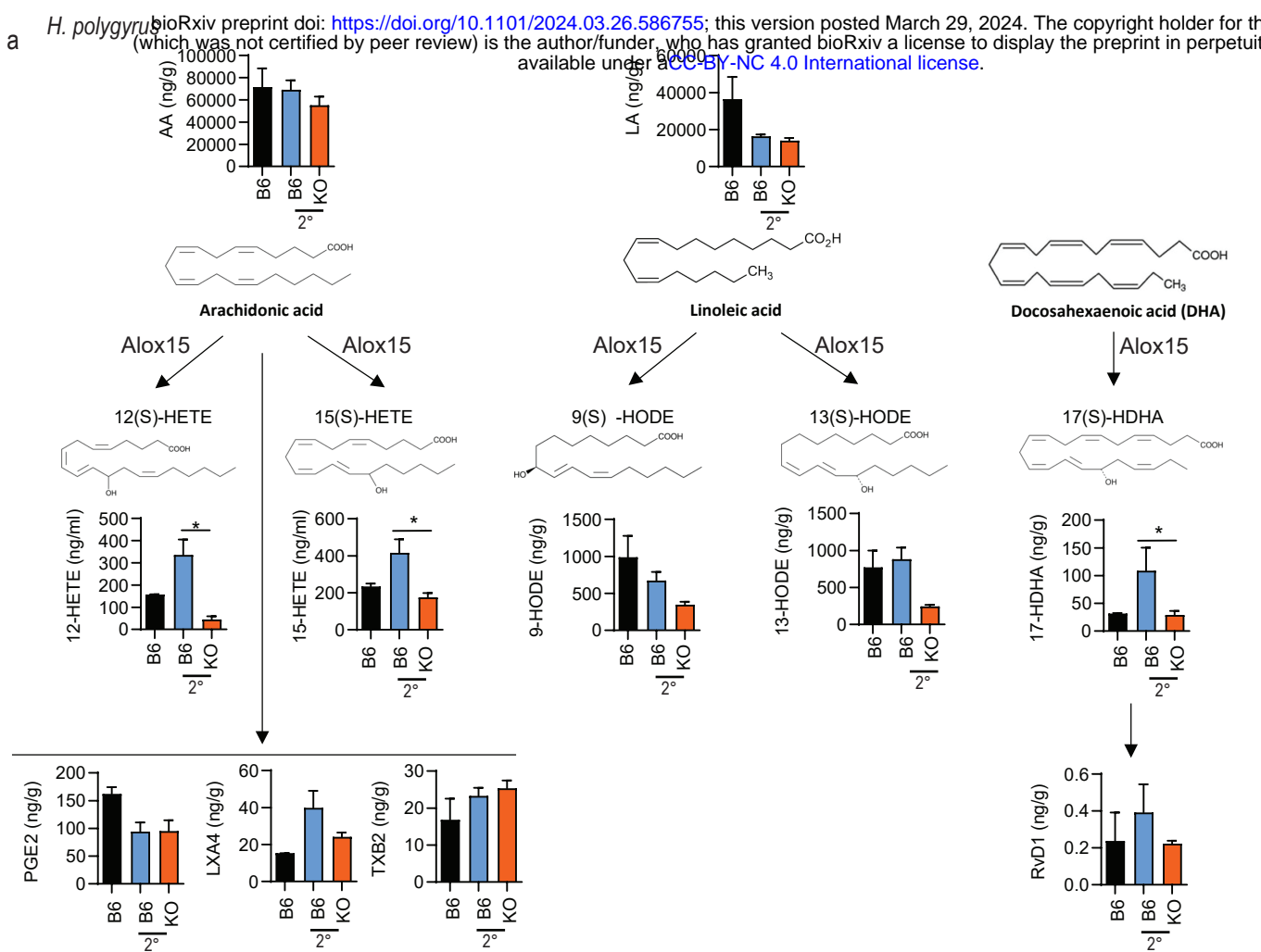
a

Figure 8: Heightened glycolysis cause loss of anti-helminth killing in Alox15-/- M2